NASA Technical Paper 1505

Evaluation of a Vortex Model of Turbulent Cavity Flow

Jay C. Hardin and P. J. W. Block

SEPTEMBER 1979

NASA

NASA Technical Paper 1505

Evaluation of a Vortex Model of Turbulent Cavity Flow

Jay C. Hardin and P. J. W. Block
Langley Research Center
Hampton, Virginia

National Aeronautics
and Space Administration

**Scientific and Technical
Information Branch**

1979

SUMMARY

A two-dimensional discrete vortex model was applied to turbulent flow over a cavity at a Reynolds number based on cavity half-length of approximately 5×10^5. These model predictions are compared with new experimental data, both on a time-average and on a spectral basis. The comparisons indicate that the vortex model reasonably reproduces the mean velocity profiles of this complex flow, while the turbulent intensity and Reynolds stress profiles are generally overpredicted in magnitude. Spectral analyses show that the vortex model introduces unrealistic low-frequency power which becomes less dominant as the model becomes more disordered. In this state, the spectral power distribution of the model is nearly in agreement with that of the data, being somewhat too low at the higher frequencies and too high at the lower frequencies. The model is also shown to be capable of reproducing the cavity feedback oscillation phenomenon. These results indicate that even in a turbulent flow, part of the flow is nearly deterministic, "determined" by the initial and boundary conditions on the flow. This is the part of the flow which is represented by such vortex models and is probably what has come to be called the "large-scale structure" of the flow. This study suggests that vortex models merit further research as a means of simulating turbulent flow and calculating the resulting noise generation.

INTRODUCTION

Computation of the noise generated by a fluid flow from the dynamic behavior of the flow itself has been a goal of the aeroacoustic community ever since the original formulation of the relevant theory by Lighthill in 1952 (ref. 1). This effort has been hampered by many factors, particularly by the fact that the acoustic sources depend on the nonlinear terms of the Navier-Stokes equations, that sound, being a dynamic process, depends on the time-varying structure of the flow, and that most flows of practical interest are random in character. Thus, it has been only recently that serious attempts to calculate sound production directly from a description of the flow itself have been made.

The major advance in the understanding of fluid mechanics which may finally make such computation feasible was the discovery (or rediscovery) of large-scale structures in a turbulent jet by Crow and Champagne (ref. 2) in the early 1970's. Since that time, such structures have also been observed in mixing layers and boundary layers over a wide range of Reynolds numbers. While the role of these structures in the generation of sound is still being debated, it is generally agreed that they are responsible for much of the dynamics of the flow itself. Thus, they allow one to approach the temporal flow description without being concerned with the total range of scales present in the complete flow; insofar as the large scales are dominant, the most important aspects of the flow can still be described.

One method of attempting to describe the large-scale flow structure has been the discrete vortex model which represents the flow vorticity by a collection of vortex singularities whose evolution is governed by the Biot-Savart law. Such models have been developed by Acton (ref. 3), Clements (refs. 4, 5, and 6), Chorin (ref. 7), Dowling (ref. 8), Davies and Hardin (ref. 9), and Leonard (ref. 10), to name but a few. Further, utilizing the equivalent of Powell's theory of vortex sound (ref. 11), several investigators (refs. 12, 13, 14, 15, and 16) have shown that sound generation by these models may easily be computed. However, such models are basically deterministic. Thus, it has not been clear exactly in what sense they model a turbulent flow field.

Experimental turbulent data and model predictions have been quantitatively compared with varying degrees of success. For example, Chorin (ref. 7) has shown good agreement between measured and predicted drag coefficients for a cylinder in uniform flow over a wide range of Reynolds numbers. Acton (ref. 3) obtained reasonable comparisons for the growth rate of a two-dimensional shear layer when the finite thickness of the layer is modeled with care. Clements and Maull (ref. 5) found good agreement for the Strouhal number and base pressure produced by vortex shedding behind a blunt-based body, although the comparison deteriorated dramatically when the base included a cavity. They also obtained fair predictions of the mean velocity profiles for flow over a step. Finally, Ashurst (ref. 17) showed that a vortex model tended to overpredict the turbulent intensities and Reynolds stress in a turbulent mixing layer, although the comparison could be greatly improved by taking the diffusion of the vortex cores into account.

In this paper, the flow field produced by such a vortex model is compared with new experimental data for high Reynolds number flow over a cavity. These data were obtained as a part of an extensive study of cavity noise generation carried out at NASA Langley Research Center (refs. 18, 19, and 20). Comparison is made on a spectral as well as on a time-average basis. This study not only assesses the validity of vortex modeling but may also aid in the understanding of the large-scale structure of turbulent flows.

The vortex model utilized in this work was developed by Hardin and Mason (ref. 14) to compute sound generated by flow over a cavity in an aerodynamic surface. This two-dimensional model is based upon a Schwarz-Cristoffel relation which transforms the cavity geometry onto a plane and thus allows the inviscid cavity flow to be obtained from the complex potential for uniform flow. The shear layer formed by flow over the cavity leading edge is then described by the insertion of discrete vortices. One vortex, whose circulation is determined by application of the Kutta condition at the leading edge, is inserted during each small time interval. The position of the vortices in the transform plane is then obtained by numerical inversion of the transformation. The boundary condition of zero normal velocity at the walls is satisfied by the inclusion of image vortices. A vortex decay function is utilized in an attempt to include the physical effects of the no slip condition. This parameter is found to be critical in order for the model to exhibit the correct mean velocity. A vorticity stretching mechanism is also employed to simulate the transfer of turbulent energy to the third dimension. The dynamic behavior of the flow can then be followed by sequential solution of the governing flow equations in time.

DEVELOPMENT OF GOVERNING EQUATIONS

Consider flow over a two-dimensional cavity as shown in figure 1, that is, a flow, which far from any surface has a free-stream velocity U_o and sweeps over a cavity of length L and depth D. This flow, of course, induces a complicated motion within the cavity which is the primary interest of this analysis.

The symbols used in this paper are defined in the appendix.

Nondimensional Equations for Flow Variables

In this analysis, where the fluid is taken to be incompressible and all variables are nondimensionalized by the free-stream velocity, cavity half-length, and fluid density, the flow field is governed by the Navier-Stokes equations:

$$\frac{\partial U_i}{\partial x_i} = 0 \tag{1}$$

and

$$\frac{\partial U_i}{\partial t} + U_j \frac{\partial U_i}{\partial x_j} = - \frac{\partial p}{\partial x_i} + \alpha \frac{\partial^2 U_i}{\partial x_j \, \partial x_j} \tag{2}$$

where U_i are the total velocity components, p is the total pressure, α is the inverse of the Reynolds number of the flow, and the Einstein summation convention is employed. These equations govern the complete flow field and can, in principle, be solved for realizations of turbulent flow regardless of the Reynolds number (ref. 21). However, this approach becomes very costly in computer resources as the Reynolds number increases (ref. 22). Thus, the only feasible approach is to employ some sort of subgrid-scale modeling (ref. 23) and to solve only for the larger scales. It is in the spirit of this type of solution that discrete vortex modeling is best understood.

Stream-Function/Vorticity Formulation

The discrete vortex technique utilizes a stream-function/vorticity formulation of the governing equations. Assume that the total flow field is two-dimensional; that is, $U_3 = 0$ and $\frac{\partial}{\partial x_3} = 0$. Then, there is only one nonzero component of vorticity in the flow:

$$\Omega = \frac{\partial U_2}{\partial x_1} - \frac{\partial U_1}{\partial x_2} \tag{3}$$

which, from equation (2), must satisfy

$$\frac{D\Omega}{Dt} = \alpha \nabla^2 \Omega \tag{4}$$

where

$$\frac{D}{Dt} = \frac{\partial}{\partial t} + U_1 \frac{\partial}{\partial x_1} + U_2 \frac{\partial}{\partial x_2}$$

and

$$\nabla^2 = \frac{\partial^2}{\partial x_1{}^2} + \frac{\partial^2}{\partial x_2{}^2}$$

If a stream function ψ is also introduced such that

$$U_1 = \frac{\partial \psi}{\partial x_2} \qquad U_2 = \frac{-\partial \psi}{\partial x_1}$$

then equation (1) is satisfied and equation (3) becomes

$$\nabla^2 \psi = -\Omega \tag{5}$$

Equations (4) and (5) represent the stream-function/vorticity formulation utilized in the discrete vortex solution technique.

DISCRETE VORTEX MODEL

The discrete vortex model utilized in this study was developed by Hardin and Mason (ref. 14) for evaluation of cavity noise production. Thus, only a brief description is included in this paper. After nondimensionalization, the cavity geometry appears as shown in figure 2(a), where $d = 2D/L$. If the complex variable $z = x + iy$ is introduced, the cavity surface may be transformed onto the real axis of the λ-plane shown in figure 2(b) by the transformation

$$z = \frac{E\left[\sin^{-1}\lambda, \sin^{-1}(1/a)\right]}{E\left[1/a^2\right]} \tag{6}$$

where $\lambda = \zeta + i\eta$, $E[\,,\,]$ is the incomplete elliptic integral of the second kind, and $E[\,]$ is the complete elliptic integral of the second kind. The points $\lambda = \pm a$ are the transforms of the exterior cavity corners at $z = \pm 1 + id$.

Solution Technique

With this transformation, the discrete vortex solution for the flow field is readily obtained. The governing equations are equations (4) and (5) which must be solved subject to the boundary conditions

$$U_1 = U_2 = 0$$

on the cavity surface. The solution uses the idea of an impulsive start (ref. 4) with the initial condition

$$U_1 = U_2 = 0$$

everywhere.

Now, for the case of interest in this paper, the Reynolds number of the flow is large; thus α (the inverse of the Reynolds number) is small. As α approaches zero, equation (4) becomes

$$\frac{D\Omega}{Dt} = 0$$

which implies that vorticity is conserved as it moves about in the flow; that is, vortical fluid tends to remain vortical. Thus, at some time t, one can imagine the flow region divided into small elements and the total vorticity in each element replaced by a discrete vortex such that the circulation around the element is conserved. These discrete vortices would then interact with each other according to the Biot-Savart law to represent the evolution of the vorticity distribution. This solution technique has been analyzed by Hald and Del Prete (ref. 24) who have shown that it converges, at least for short times, as the size of the elements is reduced.

Thus, for small α, the flow vorticity may be represented by a collection of discrete vortices

$$\Omega(x,y,t) = \sum_{i=1}^{N} \Gamma_i \, \delta(z-z_i) \tag{7}$$

where $\delta(\ )$ is the Dirac delta function, Γ_i is the circulation of the ith vortex which is located at the point $z = z_i$, and N is the number of vortices in the flow at time t. Equation (5) is then satisfied by the imaginary part of the complex potential

$$\theta(\lambda) = \beta\lambda - \frac{i}{2\pi}\sum_{i=1}^{N}\Gamma_i \ln(\lambda - \lambda_i) + \frac{i}{2\pi}\sum_{i=1}^{N}\Gamma_i \ln(\lambda - \lambda_i^*) \tag{8}$$

where λ_i are the transforms of the vortex positions z_i and

$$\beta = \frac{U_o}{a\ E\left[1/a^2\right]}$$

The first term $\beta\lambda$ is the ideal (inviscid) flow solution and the second sum consists of image vortices necessary to satisfy the condition of no flow through the cavity walls. The velocity field may then be obtained by differentiation

$$U_1 - iU_2 = \frac{d\theta}{dz}$$

and the motion of the vortices followed by numerical integration.

To satisfy the initial condition of interest, the flow is started at $t = 0$ at which time it separates at the cavity leading edge and sheds vorticity into a shear layer. At each time step Δt, this vorticity is replaced by a discrete vortex whose circulation is chosen such that the Kutta condition is satisfied at the leading edge.

This is the solution technique which was developed in reference 14. In the present analysis, three extensions of this technique have been made to better model the physics of the flow. Two of these are concerned with the viscosity of flow for which α is small but nonzero and the third with the three-dimensionality of the flow.

Models for Flow Physics

The first extension results from an idea of Chorin (ref. 7). For nonzero viscosity, equation (4) is just a diffusion equation in a moving medium. Thus, in each time step Δt, the effect of the right side may be approximated by

adding to the motion of the vortices small random displacements Δx and Δy such that

$$\langle \Delta x \rangle = \langle \Delta y \rangle = 0$$

and

$$\langle \Delta x^2 \rangle = \langle \Delta y^2 \rangle = 2\alpha \, \Delta t$$

where $\langle \rangle$ is the expectation operator. This technique leads to a tighter rollup of the initial vortex sheet and has been shown to yield better agreement with experiment (ref. 17).

The second extension of reference 14 was suggested by the observation that the no slip condition on the cavity walls cannot be satisfied by this semi-inviscid solution technique. In actuality, this condition causes positive vorticity to be generated along the walls of the cavity which tends to cancel out some of the large negative vorticity produced in the shear layer. In an attempt to include this effect in a simple fashion, the circulation of each of the discrete vortices was taken to be a function of time

$$\Gamma_i(t) = \Gamma_i(t_i) + K(t - t_i) \tag{9}$$

where t_i is the time at which the ith vortex was formed, $\Gamma_i(t_i)$ is the initial circulation determined from the Kutta condition, and K is the circulation decay rate. When the circulation becomes zero, the vortex is removed from the calculation. This parameter also models, in a sense, the viscous dissipation of turbulent energy in the flow.

The final change in the model of reference 14 attempts to account, in an elementary fashion, for the three-dimensionality of the flow. Since in two dimensions, the vortex stretching term of the Helmholtz equation is identically zero, there is no mechanism in the model for the transfer of energy to the third dimension. However, in reality, the vortices formed by the shear layer over the cavity are not infinitely long, but have length equal to the cavity width W and are bounded by the cavity walls. Such a finite-length vortex does not generate the same velocity at all points equidistant from it, as does a vortex filament. In fact, for the geometry of figure 3(a), it can be shown that the velocity V induced by the vortex segment at the point P is given by

$$V = \frac{\Gamma}{4\pi h}(\cos \alpha' + \cos \beta')$$

Now, suppose two straight vortex segments, say n and k, are initially separated by a distance h. Over a small time interval Δt, the velocity induced on vortex k by vortex n stretches vortex k into a curved shape as shown in figure 3(b). From equation (9), it can be determined that the center point of vortex k has moved a distance ℓ farther than its end points where

$$\ell = \frac{\Gamma_n}{4\pi h}\left\{\frac{2}{\left[1 + (2h/W)^2\right]^{1/2}} - \frac{1}{\left[1 + (h/W)^2\right]^{1/2}}\right\}\Delta t \approx \frac{\Gamma_n \Delta t}{4\pi h} \tag{10}$$

for $h << W$. Thus, the vorticity of vortex k, which was originally all in the direction of the cavity width, now has components in both that direction and in the xy-plane, as shown in figure 3(b). The effect of this energy transfer is included in the model by reevaluating the circulation of each vortex at every time step through the relation developed with the help of equation (10),

$$\Gamma_k(t+\Delta t) = \Gamma_w = \Gamma_k(t)\frac{W}{2\left[\left(\frac{W}{2}\right)^2 + \left(\frac{\Gamma_n \Delta t}{4\pi h}\right)^2\right]^{1/2}} \tag{11}$$

where the nth vortex is taken as the one closest to vortex k and h is the distance between them. The small component of vorticity in the xy-plane is neglected in subsequent calculations. Note that equation (11) has an effect similar to that of equation (9), but arises through a different physical mechanism.

EXPERIMENTAL RESULTS

The flow measurements around the cavity were performed in the open jet anechoic flow facility at the NASA Langley aircraft noise reduction laboratory in conjunction with acoustic measurements. The cavity apparatus is shown in figure 4. It has a continuously variable streamwise length L, two values for the depth D of 3.19 cm and 5.11 cm, and a fixed width W of 5.08 cm. The variable length for each of these depths was accomplished by the sliding blocks shown in figure 4. The cavity apparatus was set in a 1.25-cm-thick tempered aluminum plate, depicted in figure 5, which was curved downstream of the cavity to eliminate trailing-edge noise effects. The plate was flush with the lower lip of the nozzle (seen also in fig. 4). The leading edge of the cavity was about 5.5 cm from the lip of the nozzle which measured 30 cm by 45 cm. Nozzle exit Mach number varied from 0.116 to 0.362. The turbulence intensity in the nozzle flow was about 1 percent. The velocity profile at the nozzle exit had less than a 1.5-percent overshoot and a boundary-layer thickness of 0.5 cm at the maximum velocity. This corresponds to a 0.61-cm thickness at the leading

edge of the cavity, assuming a turbulent boundary layer progressing over a flat plate. The corresponding momentum thickness is 0.059 cm. This agrees with the momentum thickness which was calculated from the mean velocity profile for this velocity near the leading edge of the cavity.

Table I lists the cavity configurations, test Mach numbers, and measurement locations for the velocity surveys. The five cases, or cavity configurations, represented three values of length-to-depth ratio: 0.78 for a rather deep cavity, 5.01 for a relatively shallow cavity, and 2.35 as an intermediate value. Data were obtained at three velocities for each of these cases. Flow profiles were obtained in the middle of the cavity width near the leading and trailing edges except for cases 1 and 3 where only the leading-edge profiles were obtained. The positions of the velocity surveys are given in the last two columns of table I in terms of the distance in centimeters from the leading edge of the cavity.

A cross-wire (x-shaped hot-wire) anemometer was used to measure the velocity profiles. The wires were platinum-plated tungsten, 0.0038 mm in diameter and 1.25 mm in length, and were operated in the linearized constant-temperature mode. Time histories of the x- and y-components of the velocity were recorded and subsequently analyzed by computer. The data were corrected according to reference 25 for errors due to turbulence nonlinearities and irregular cooling (not following the cosine law). The error in the mean measurements is less than 3 percent. Results presented include mean velocity profiles, turbulence intensity profiles, and mean Reynolds stress profiles for each case and test velocity. A few spectra are also presented. These results are normalized by the free-stream velocity U_o which was taken to be the jet exit velocity.

The mean velocity profiles are shown in figure 6. When normalized by the free-stream velocity, the profiles for a particular case and streamwise position are generally independent of Mach number, the exception being at the trailing edge for case 2. Evidently, the values exceeding $\bar{U}_1/U_o = 1$ indicate that the velocity overshoots its asymptotic value which would be measured at larger values of Y. Near the leading edge, the mean velocity at $Y/D = 1$ is nominally $0.55U_o$; near the trailing edge, this value increases to $0.65U_o$. Although the shear flow inside the cavity is developing and cannot strictly be considered self-similar, the spreading rate determined from the mean velocity profiles near the leading and trailing edges is consistent with that for self-similar shear layers as given in reference 26.

The turbulence intensity profiles are given in figure 7. The leading-edge measurements for cases 1 and 3 are shown in figure 7(a). For these two cases, where the cavity length is small (or where the cavity is considered deep), the profiles of the streamwise and cross-stream turbulent velocity fluctuations, u_1 and u_2 respectively, have the same shape with the maximum occurring at $Y/D = 1$. For cases, 2, 4, and 5, shown in figures 7(b), 7(c), and 7(d), respectively, the u_2 profiles at the leading edge are similar to those obtained in cases 1 and 3 in that the maximum value occurs at $Y/D = 1$. However, the u_1 profile departs from this shape at the leading edge by maintaining high levels of turbulence intensity down into the cavity. At the leading edge, the the maximum turbulence intensity level for all cases is nominally 9 percent.

At the trailing edge, the cross-stream turbulence intensity level reaches 13 percent at $Y/D = 1$, while the streamwise turbulence intensity level ranges from 15 percent to 20 percent.

The mean Reynolds stress profiles are given in figure 8. At the leading edge, the maximum always occurs at $Y/D = 1$. At the trailing edge, the location of the maximum (negative) value varies from outside to inside the cavity depending on the velocity and cavity configuration.

Since the turbulence intensity levels and mean velocity profile shape change with cavity configuration and, sometimes, with free-stream velocity, it is difficult to make comparisons with data obtained in cavities of differing configuration and test conditions. However, it should be pointed out that the measurements reported herein are consistent with those of reference 27 in that the profiles agree and the levels fall in the same range. Reference 27 contains the only other measurements of the turbulence intensity profiles inside the cavity that the authors found.

The spectral densities of the velocity fluctuations obtained from the recorded time histories for case 2 at 124 m/s are shown in figure 9. These results are typical of the spectra measured in the cavity. The analysis bandwidth for these spectra is 30 Hz and each spectrum has at least 240 degrees of freedom. Outside the cavity ($Y/D = 1.45$), the tonal aspects of the feedback phenomenon are clearly seen in both the u_1 and u_2 spectra. As the hot-wire probe descends into the cavity, the spectra take on a more broadband appearance, although the u_2 spectra remain predominantly peaked. The maximum root-mean-square values of the velocity occur when $Y/D = 1$. Inside the cavity ($Y/D = 0.6$), the tonal appearance of the spectra has faded in relation to the broadband spectra of the turbulent flow.

COMPARISON OF MODEL RESULTS WITH EXPERIMENT

The experimental case chosen for comparison with the vortex model is case 2 of table I at the highest velocity of 124.2 m/s. For these data, $L/D = 2.35$ which is in the range of values most commonly seen in aircraft applications. Further, the Reynolds number based on the cavity half-length is approximately 5×10^5 which approaches that found on an aircraft during landing approach.

The vortex model was programmed for the parametric values corresponding to this case and run for 1000 time steps with a nondimensional step size $\Delta t = 0.05$. This step size has been shown by previous work to be a reasonable compromise between integration accuracy and computation time. Figure 10 shows an instantaneous realization of the flow field for a particular value of nondimensional time after the stationary state has been achieved. The symbols in this figure are cross sections of the rectilinear vortices. Note that the shear layer, which is initially represented by a linear array of vortices, becomes unstable and breaks up into coherent masses of vorticity which are easily discernible. These large-scale structures are then swept downstream to impinge on the trailing edge of the cavity. Also shown in the figure are the two locations at which the experimental data were taken to give the reader a physical feeling for the vortex model near these two positions.

Mean Velocity Profiles

In figure 11, the mean velocity profiles predicted by the vortex model at the two measurement locations are compared with the experimental data. The vortex model results were obtained by first allowing the model to run until a steady state was achieved and then calculating time histories of the velocity components U_1 and U_2 at the points of interest through differentiation of equation (8). These were then time-averaged to obtain estimates of the mean velocities $\bar{U}_1$ and $\bar{U}_2$. As can be seen, there is reasonable agreement between the data and predictions except within the cavity itself at the trailing-edge position where the streamwise velocity component is underpredicted and the cross-stream component is overpredicted. The reason for this discrepancy appears to be the three-dimensionality of the flow within the cavity.

The value of the circulation decay rate constant K in equation (9) was chosen to make the $\bar{U}_2$ velocity component of the vortex model match the data at $2X/L = -0.85$ and $Y/D = 1.0$. The ideal fluid solution for the cavity flow (the first term in equation (8)) results in a negative $\bar{U}_2$ velocity component in this region. As can be shown from equation (8), in the vortex model this negative velocity is opposed by a positive velocity component induced by the high vorticity in the cavity. These must balance to yield the near zero value seen in the experimental data. This necessary balance is rather delicate, and thus the model is quite sensitive to the value of K employed. The value used in the model, $K = 0.00125$, was found by trial and error and did not quite make the velocity match, as seen in figure 11.

Turbulent Intensity Profiles

In figure 12, the turbulent intensity profiles predicted by the vortex model are compared with the experimental data. The values for the vortex model were again obtained by time-averaging the squared difference between the steady-state velocity values and the appropriate mean velocities; that is, $\overline{u_i^2} = \overline{(U_i - \bar{U}_i)^2}$. As can be seen, the shapes of the profiles are generally similar except that the predicted profiles at the trailing-edge position peak slightly below the top of the cavity, while the data peak at the top of the cavity. The predicted intensity levels are reasonable above the cavity, but tend to be too high by about a factor of 2 within the cavity itself. This is thought to be because the true three-dimensional character of the flow in the cavity has not been well represented by the model. It was assumed that the incorporation of equation (11) would help to alleviate this problem. However, it had negligible effect except to reduce the value of the circulation decay constant K required to obtain the correct velocity profiles.

High peaks in intensity can be seen in the predicted profiles at the level of the cavity at the leading-edge position. The major reason for these peaks is that many of the vortices being released from the leading edge of the cavity pass quite close to the point where the velocity is being calculated, as can be seen in figure 10. Thus, the singular nature of the vortices causes quite high velocity fluctuations. In an attempt to remedy this situation, the vortices were assumed to have a finite core. If the point of interest fell within the

core of one of the vortices, the velocity at the point was then computed using Routh's rule (eq. (9) of ref. 14). As can be seen in figure 12, this attempt was not entirely successful. The nondimensional vortex core size, used in all the calculations in this paper, was 0.002.

However, as will be seen later, the spectra at the leading-edge position are dominated by low-frequency power, apparently induced by this vortex singularity problem. Also shown in figure 12 are intensity values obtained by high-pass filtering the signals at 110 Hz. Filtering dramatically reduces the high values at the level of the cavity at the leading-edge position, while generally leading to better agreement with the data elsewhere.

In figure 13, the predicted Reynolds stress profiles, $\overline{u_1 u_2}$, at both measurement locations are compared with the experimental data. As can be seen, both the shapes and levels agree reasonably well except at the level of the cavity at the leading-edge position. Here again a large peak appears in the model, undoubtedly caused by the low-frequency power.

Spectra

Also of interest are comparisons of the vortex model with the data on a spectral basis, particularly since the model was developed to calculate noise which depends strongly on the time-dependent behavior of the flow. The major difficulty with such an endeavor, however, is to obtain sufficient computed values to yield an accurate spectral estimate; more computer time is required as the number of vortices increase. As mentioned before, the model was computed with a nondimensional step size of $\Delta t = 0.05$ which had been chosen to allow accurate determination of the vortex paths. For the case considered, this corresponds to a dimensional time step $\Delta T = 24.1$ μs and Nyquist frequency of approximately 21 kHz. Direct spectral analysis of these records produced spectra with very little power above 7 kHz in agreement with the experimental data. Thus, it became apparent that records with a step size of $3\ \Delta T$ were adequate to estimate the spectra, even though this meant discarding two-thirds of the computed values. At the leading-edge measurement location, record lengths of 1000 values were obtained. The first 232 of these values were discarded as being nonstationary and every third value of the last 768 were selected to provide one record of 256 values with a step size of $3\ \Delta T$. This record was analyzed by the fast Fourier transform (FFT) technique to provide a spectral estimate with 2 degrees of freedom, a Nyquist frequency of approximately 7 kHz, and a bandwidth of approximately 50 Hz. At the trailing-edge location, record lengths of 2000 values were obtained. The first 464 of these values were discarded as being nonstationary and every third value of the last 1536 was selected to provide 4 consecutive records of 128 values. These records were again analyzed by the FFT to yield spectral estimates with 8 degrees of freedom, a Nyquist frequency of approximately 7 kHz, and a bandwidth of approximately 100 Hz. Typical spectra so obtained are shown in figure 14. These are spectra of the streamwise velocity component at $2X/L = 0.65$ for three different values of Y/D. Obviously, these spectra are highly variable as one would expect for spectral estimates with so few degrees of freedom. However, these spectra are reasonably similar and appear to contain consistent peaks in the frequency range from 0.6 to 3 kHz.

As can be seen in figure 9, the experimental data also show reasonably similar spectra at both the leading- and trailing-edge positions. Thus, to reduce the variability of the spectra predicted by the vortex model and to better define any peaks which might be present, it was determined to normalize each spectrum by its mean square value and to average together all spectra for a particular velocity component at a particular downstream location. Insofar as these records are independent, this averaging nominally yields spectra with 10 degrees of freedom at the leading-edge location and 72 degrees of freedom at the trailing-edge location.

Figures 15(a) and 15(b) show the resulting spectra at the two measurement locations. Note that there is also considerable similarity between the spectra of the streamwise and cross-stream velocity components. At the leading-edge location, where the vortex model is rather orderly (see fig. 10), the spectra are dominated by tremendous low-frequency (<0.3 kHz) power, as mentioned previously. This is apparently an artifact of the vortex model due to representing the finite-thickness shear layer as an infinitesimal sheet. On the other hand, at the trailing-edge location, where the vortex model has become more disordered, the low-frequency power is much less dominant and distinct peaks are present in the spectra similar to those observed in the experimental data of figure 9.

The presence of these tones in the experimental data is a result of the well-known self-sustaining oscillation of flow past cavities. This phenomenon has been observed for many years and recently has been the subject of an excellent review by Rockwell and Naudascher (ref. 28). This oscillation is presently understood in terms of a feedback mechanism. Vorticity is shed from the leading edge of the cavity and convects down the length of the cavity at some convection speed U_c until it impinges on the trailing edge. An acoustic wave travels back upstream at the speed of sound and, upon reaching the leading edge, causes more vorticity to be shed. This explanation led Block (ref. 18) to develop the relation,

$$N_{Str} = \frac{n}{\frac{1}{K_V} + M\left(1 + \frac{0.514}{L/D}\right)} \qquad (n = 1, 2, 3, \ldots) \qquad (12)$$

for the Strouhal numbers at which the oscillations occur. Here n is the mode number and $K_V = U_C/U_O$ is the convection velocity ratio. This expression agreed well with the tones observed in the far-field sound spectra radiated by the cavity (ref. 19), which occur at the same frequencies as the cavity flow oscillation phenomenon.

Of course, the vortex model is incompressible, resulting in an infinite speed of sound, or conversely, an effective Mach number of zero. Thus, one would expect the acoustic half of the feedback loop in the model to occur instantaneously, so that from equation (12), the following simple relation for the expected frequencies results:

$$f_n = n \frac{U_o}{L} K_v = \frac{nU_c}{L} \qquad (n = 1, 2, 3, \ldots) \qquad (13)$$

Taking $U_c = 0.6U_o$, the value most commonly employed, yields the frequencies shown at the bottom of figure 15(b) for the first four oscillation frequencies. Ordinarily only the first four can be observed experimentally (ref. 19). These frequencies are harmonics with the fundamental occurring at about 0.62 kHz.

As can be seen from the spectra of figure 15(b), the vortex model also exhibits preferred frequencies in this range. In fact, a fundamental frequency close to 0.7 kHz and its first three harmonics appear to be present as well as an unexplained oscillation near 1 kHz. As there can be little doubt that these peaks are real, since the spectral estimates have approximately 72 degrees of freedom, the vortex model does appear to predict the self-sustaining oscillation phenomenon of the cavity, as speculated by Rockwell and Naudascher (ref. 28). However, the frequencies are slightly shifted.

In figure 16, the spectral densities of the dimensional (nonnormalized) streamwise velocity fluctuations as measured and as predicted by the model are compared at $2X/L = 0.65$ and $Y/D = 1.35$. This point was chosen as one where the mean square velocity fluctuations (integral of the spectrum) predicted by the model nearly agreed with those measured, and thus the frequency comparison would not be distorted by differences in power levels. As can be seen, the vortex model tends to underpredict the spectral levels at the higher frequencies which is compensated by an overprediction at the lower frequencies. This is to be expected since there is no mechanism in the vortex model for the cascade of energy to higher wave numbers that occurs in true turbulent flows. Other than this power "tilt" and the shift in the peak frequencies due to incompressibility, the spectral shapes are reasonably similar. This result encourages further research into the use of vortex models to simulate turbulence and to calculate the resulting noise radiation, particularly if the physics of the energy cascade can be built into the model in some fashion.

Finally, with regard to the turbulent energy spectrum, it is of interest to determine the effect of the circulation decay rate constant K on the distribution of turbulent energy. Recall that the mean velocity profiles were very sensitive to the value of this parameter. Figures 17(a) and 17(b) show the normalized spectra of the streamwise and cross-stream velocity fluctuation components at $2X/L = 0.65$ for two values of the decay rate constant: $K = 0.00125$, the value used in the model, and $K = 0.000625$, one-half the previous value. Since the mean velocity is critically dependent upon K, the flow in the latter case is far from correct. However, it can be seen that the overall spectral shapes are the same, the only difference being a shift in the tonal frequencies. Thus, it can be concluded that the circulation decay rate parameter has very little effect on the distribution of turbulent energy.

CONCLUSIONS

A vortex model of turbulent flow in a rectangular cavity has been developed and subjected to extensive comparison with experimental data. This study has resulted in the following conclusions:

1. When vorticity generation on the walls of the cavity is taken into account, the vortex model does reasonably well in predicting the mean velocity profiles of the turbulent cavity flow, particularly in regions where the flow is essentially two-dimensional. The prediction deteriorates in regions where the flow becomes more fully three-dimensional.

2. The vortex model tends generally to overpredict the turbulent intensities, again being more accurate in regions where the flow is nearly two-dimensional but high by a factor of approximately 2 as three-dimensional effects become important. This characteristic should be greatly improved if a means for energy transfer to the third dimension could be included in the model in a computationally efficient manner.

3. The vortex model contains unrealistic low-frequency power, especially where the model is orderly. The importance of this power is greatly diminished as the model becomes disordered.

4. The vortex model appears capable of reproducing flow phenomena such as the cavity feedback oscillation. However, frequencies are changed by the incompressible nature of the model.

5. The spectral distribution of power predicted by the model is quite reasonable when the model is disordered. There is a tendency for overprediction at lower frequencies and underprediction at higher frequencies because the model does not include an energy cascade mechanism.

Overall, this study indicates that vortex models merit further research as means of simulating turbulent flow and of calculating the resulting noise generation. The most crucial area for further research is inclusion of three-dimensionality and energy cascade in a computationally efficient manner. Finally, the similarity between the vortex model results and the actual measurements in a turbulent flow suggests that a part of the turbulent flow is nearly deterministic, "determined" by the initial and boundary conditions for the flow. For example, every realization of the turbulent cavity flow includes a large vortex within the cavity itself. It is this large-scale behavior of the flow which is being reproduced by the vortex model - quite possibly the same behavior that has come to be called the "large-scale structure" of the flow.

Langley Research Center
National Aeronautics and Space Administration
Hampton, VA 23665
July 20, 1979

APPENDIX

SYMBOLS

D	cavity depth
$E[\,]$	complete elliptic integral of second kind
$E[\,,\,]$	incomplete elliptic integral of second kind
K	circulation decay rate
K_v	convection velocity ratio
L	cavity length
M	Mach number
N	number of vortices in flow
N_{Str}	Strouhal number
P	point in space
S_{ii}	spectral density of velocity fluctuations in i-direction
T_a	ambient temperature
U_c	convection speed
U_i	total velocity components
U_o	free-stream velocity
V	velocity induced by vortex segment
W	cavity width
X,Y	dimensional Cartesian coordinates
a	position of transformed cavity corner
d	nondimensional cavity depth
f_n	frequency of mode n
h	normal distance
ℓ	displacement distance
n	mode index

APPENDIX

p	total pressure
p_a	ambient pressure
t	time
u_i	fluctuating velocity components
x_i	Cartesian coordinates
x,y	nondimensional Cartesian coordinates
z	complex variable
α	inverse of Reynolds number
α'	angle
β	constant in transformation
β'	angle
Γ_i	circulation of ith vortex
Γ_w	circulation in direction along width of cavity
Γ_{xy}	circulation in xy-plane
ΔT	dimensional time step
Δt	nondimensional time step
$\Delta x, \Delta y$	random displacements
ζ,η	Cartesian coordinates in transform plane
θ	complex potential
λ	complex variable
ψ	stream function
Ω	total vorticity
$\overline{\quad}$	time average
$< >$	ensemble average
$*$	complex conjugate

REFERENCES

1. Lighthill, M. J.: On Sound Generated Aerodynamically. I. General Theory. Proc. R. Soc. (London), ser. A, vol. 211, no. 1107, Mar. 20, 1952, pp. 564-587.

2. Crow, S. C.; and Champagne, F. H.: Orderly Structure in Jet Turbulence. J. Fluid Mech., vol. 48, pt. 3, Aug. 16, 1971, pp. 547-591.

3. Acton, E.: The Modelling of Large Eddies in a Two-Dimensional Shear Layer. J. Fluid Mech., vol. 76, pt. 3, Aug. 11, 1976, pp. 561-592.

4. Clements, R. R.: An Inviscid Model of Two-dimensional Vortex Shedding. J. Fluid Mech., vol. 57, pt. 2, Feb. 6, 1973, pp. 321-336.

5. Clements, R. R.; and Maull, D. J.: The Representation of Sheets of Vorticity by Discrete Vortices. Prog. Aerosp. Sci., vol. 16, no. 2, 1975, pp. 129-146.

6. Clements, R. R.: Flow Representation, Including Separated Regions, Using Discrete Vortices. Computational Fluid Dynamics AGARD-LS-86, 1977, pp. 5-1 - 5-20.

7. Chorin, Alexandre Joel: Numerical Study of Slightly Viscous Flow. J. Fluid Mech., vol. 57, pt. 4, Mar. 6, 1973, pp. 785-796.

8. Dowling, Ann P.: The Refraction of Sound by a Shear Layer Made up of Discrete Vortices. R. & M. No. 3770, British A.R.C., 1975.

9. Davies, P. O. A. L.; and Hardin, J. C.: Potential Flow Modelling of Unsteady Flow. Univ. of Southampton paper presented at International conference on Numerical Methods in Fluid Dynamics (Southampton, England), Sept. 1973.

10. Leonard, A.: Simulation of Three-Dimensional Separated Flows With Vortex Filaments. Proceedings of the Fifth International Conference on Numerical Methods in Fluid Dynamics, Volume 59 of Lecture Notes in Physics, A. I. van de Vooren and P. J. Zandbergen, eds., Springer-Verlag, 1976, pp. 280-284.

11. Powell, Alan: Theory of Vortex Sound. J. Acoust. Soc. America, vol. 36, no. 1, Jan. 1964, pp. 177-195.

12. Davies, P. O. A. L.; Hardin, J. C.; Edwards, A. V. J.; and Mason, J. P.: A Potential Flow Model for Calculation of Jet Noise. Aeroacoustics: Jet Noise, Combustion and Core Engine Noise, Ira R. Schwartz, ed., Volume 43 of Progress in Astronautics and Aeronautics, Martin Summerfield, series ed., American Inst. Aeronaut. & Astronaut., c.1976, pp. 91-106.

13. Hardin, Jay C..: Analysis of Noise Produced by an Orderly Structure of Turbulent Jets. NASA TN D-7242, 1973.

14. Hardin, Jay C.; and Mason, Jean P.: Broadband Noise Generation by a Vortex Model of Cavity Flow. AIAA J., vol. 15, no. 5, May 1977, pp. 632-637.

15. Hardin, Jay C.: Noise Calculation on the Basis of Vortex Flow Models. Noise and Fluids Engineering, Robert Hickling, ed., American Soc. Mech. Eng., c.1977, pp. 59-67.

16. Yates, John E.: Interaction With and Production of Sound by Vortex Flows. AIAA Paper No. 77-1352, Oct. 1977.

17. Ashurst, W. T.: Numerical Simulation of Turbulent Mixing Layers Via Vortex Dynamics. SAND77-8613 (Contract AT (29-1) 789), Sandia Lab., Feb. 1977.

18. Block, Patricia J. W.: Noise Response of Cavities of Varying Dimensions at Subsonic Speeds. NASA TN D-8351, 1976.

19. Block, P. J. W.: Measurements of the Tonal Component of Cavity Noise and Comparison With Theory. NASA TP-1013, 1977.

20. Tam, Cristopher K. W.; and Block, Patricia J. W.: On the Tones and Pressure Oscillations Induced by Flow Over Rectangular Cavities. J. Fluid Mech., vol. 89, pt. 2, Nov. 28, 1978, pp. 373-399.

21. Orszag, Steven A.; and Patterson, G. S., Jr.: Numerical Simulation of Turbulence. Statistical Models and Turbulence, Vol. 12 of Lecture Notes in Physics, M. Rosenblatt and C. Van Atta, eds., Springer-Verlag, 1972, pp. 127-147.

22. Fox, Douglas G.; and Lilly, Douglas K.: Numerical Simulation of Turbulent Flows. Rev. Geophys. & Space Phys., vol. 10, no. 1, Feb. 1972, pp. 51-72.

23. Deardorff, J. W.: The Use of Subgrid Transport Equations in a Three-Dimensional Model of Atmospheric Turbulence. Trans. ASME Ser. I: J. Fluids Eng., vol. 95, no. 3, Sept. 1973, pp. 429-438.

24. Hald, Ole; and Del Prete, Vincenza Mauceri: Convergence of Vortex Methods for Euler's Equations. Math. Comput., vol. 32, no. 143, July 1978, pp. 791-809.

25. Champagne, F. H.; and Sleicher, C. A.: Turbulence Measurements With Inclined Hot-Wires - Part 2. Hot Wire Response Equations. J. Fluid Mech., vol. 28, pt. 1, Apr. 12, 1967, pp. 177-182.

26. Wygnanski, I.; and Fiedler, H. E.: The Two-Dimensional Mixing Region. J. Fluid Mech., vol. 41, pt. 2, Apr. 13, 1970, pp. 327-361.

27. Tani, Itiro; Iuchi, Matsusaburo; and Komoda, Hiroyuki: Experimental Investigations of Flow Separation Associated With a Step or a Groove. Rep. No. 364, Aeronaut. Res. Inst., Univ. of Tokyo, Apr. 1961.

28. Rockwell, D.; and Naudascher, E.: Review - Self-Sustaining Oscillations of Flow Past Cavities. Trans. ASME, Ser. I: J. Fluids Eng., vol. 100, no. 2, June 1978, pp. 152-165.

TABLE I.- TEST CONDITIONS FOR VELOCITY SURVEYS

[T_a = 18.3° C, p_a = 761.2 mm Hg[a]]

Case	Cavity dimensions, cm			L/D	Test Mach numbers			Position of vertical survey, cm from leading edge	
	L	W	D					Leading-edge position	Trailing-edge position
1	4.0	5.08	5.11	0.78	0.116	0.226	0.362	0.9	----
2	12.0	↓	5.11	2.35	.146	.246	↓	↓	9.9
3	2.5		3.19	.78	.116	.246			----
4	7.5		3.19	2.35	.116	.246			6.2
5	16.0		3.19	5.01	.146	.316			14.6

[a]1 mm Hg = 133 Pa.

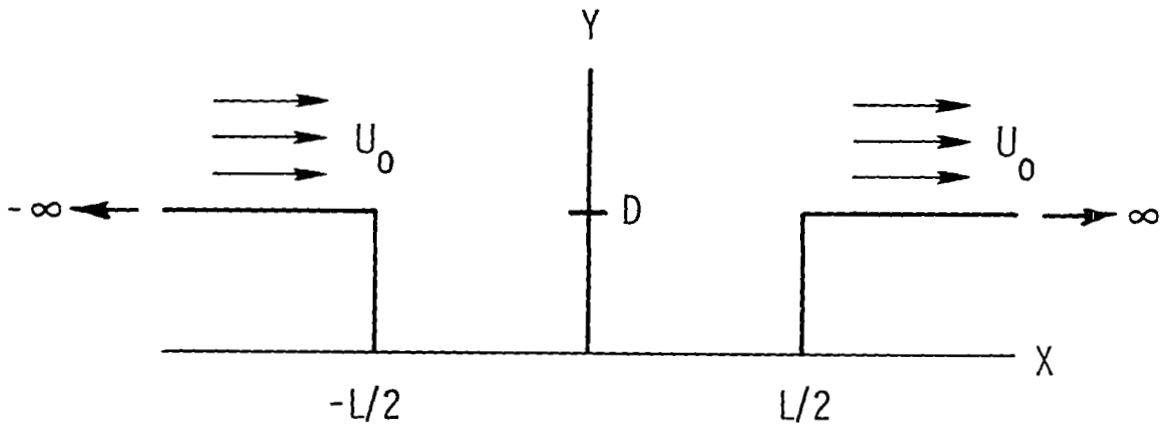

Figure 1.- Cavity geometry.

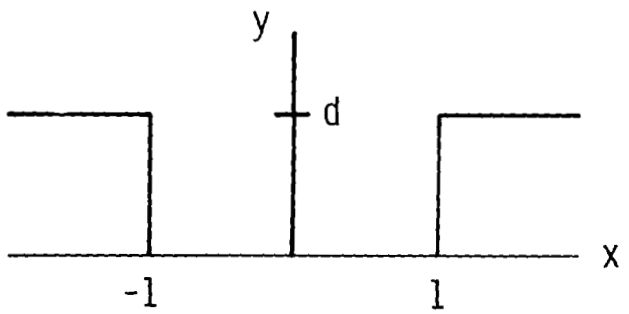

(a) z-plane.

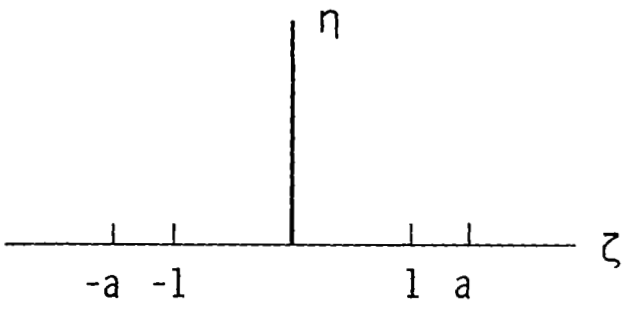

(b) λ-plane.

Figure 2.- Cavity geometry transformation.

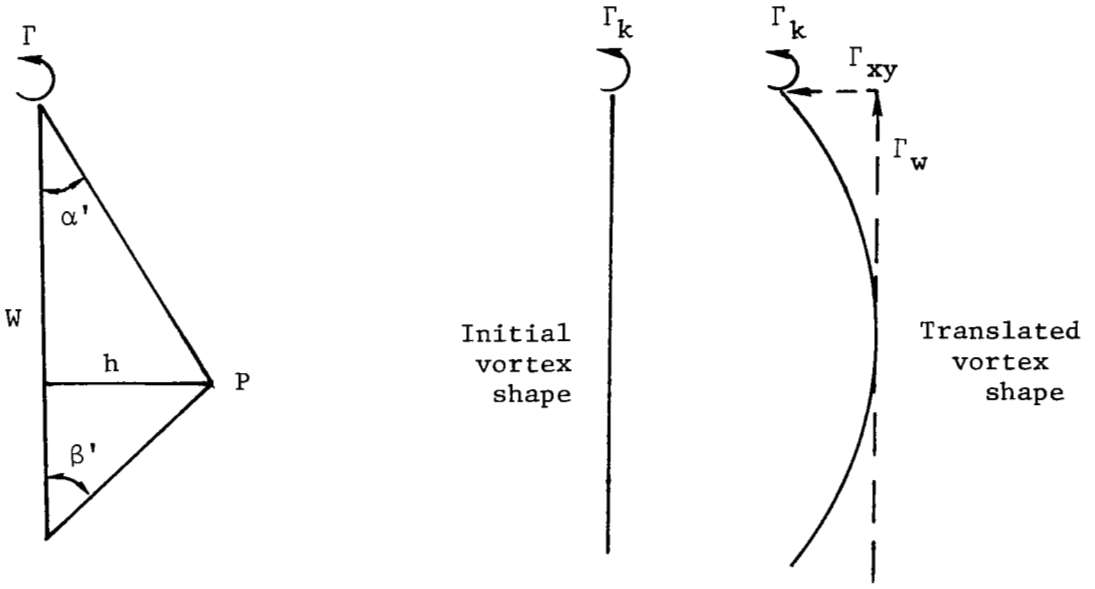

(a) Geometry of finite length vortex.

(b) Distortion of vortex by induced velocity field.

Figure 3.- Effect of finite length of vortices.

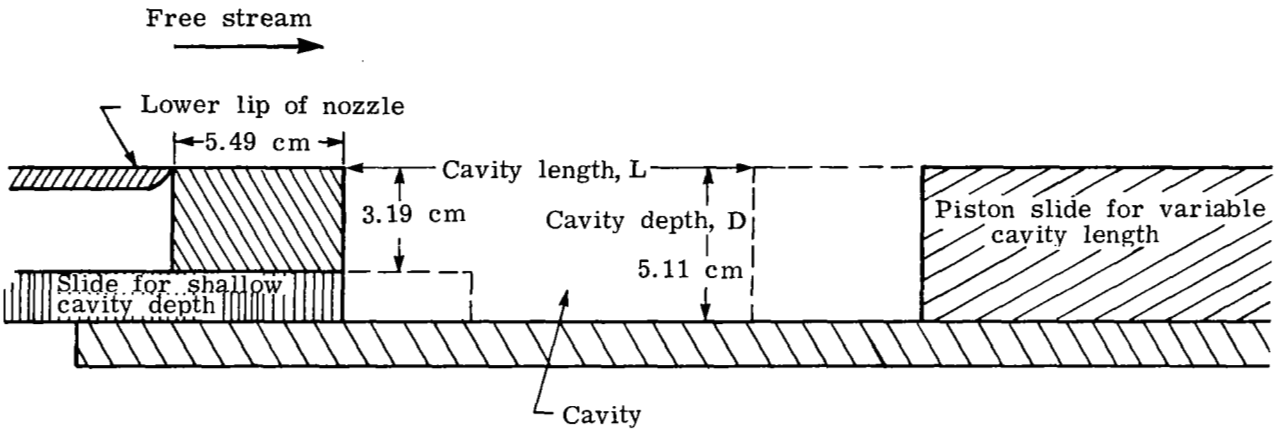

Figure 4.- Cross-sectional view of cavity apparatus.

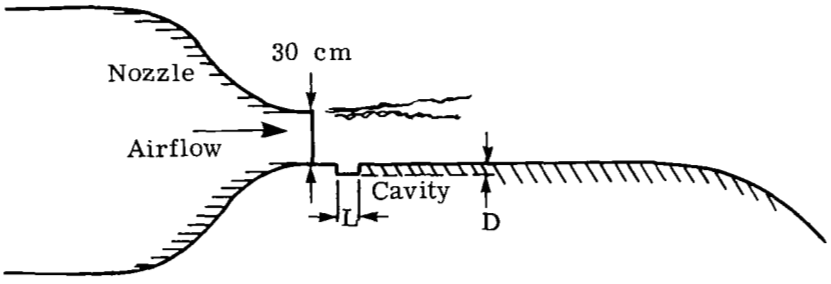

Figure 5.- Schematic drawing of cavity apparatus in open-jet anechoic flow facility.

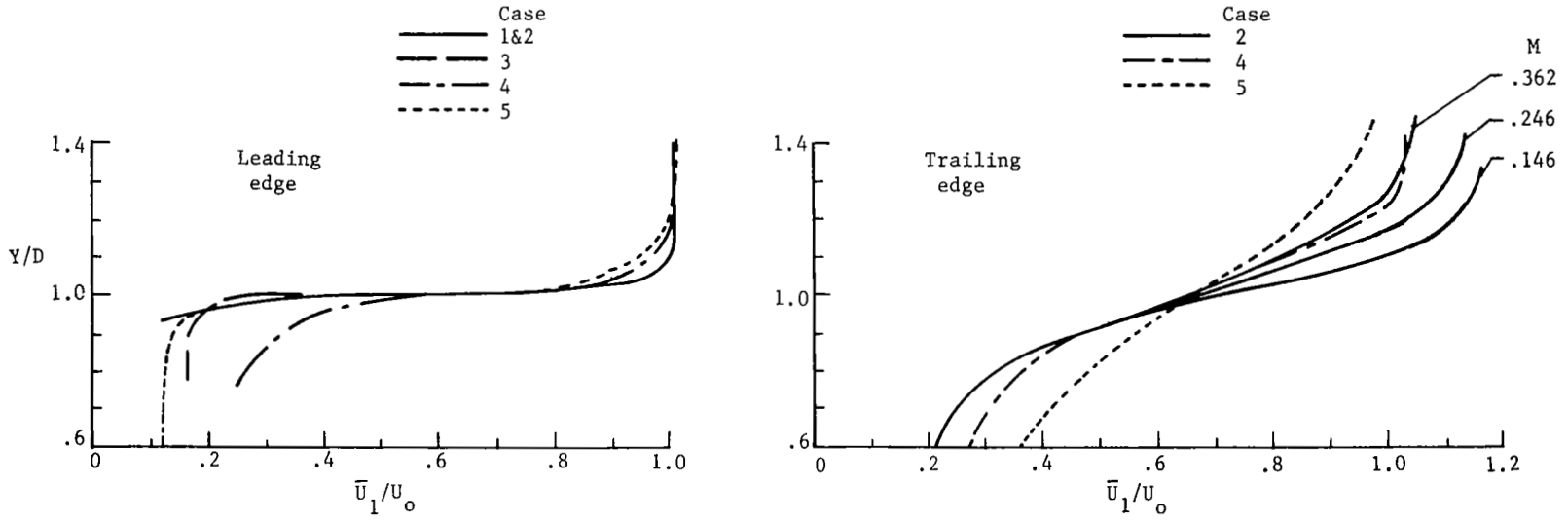

Figure 6.- Mean velocity profiles.

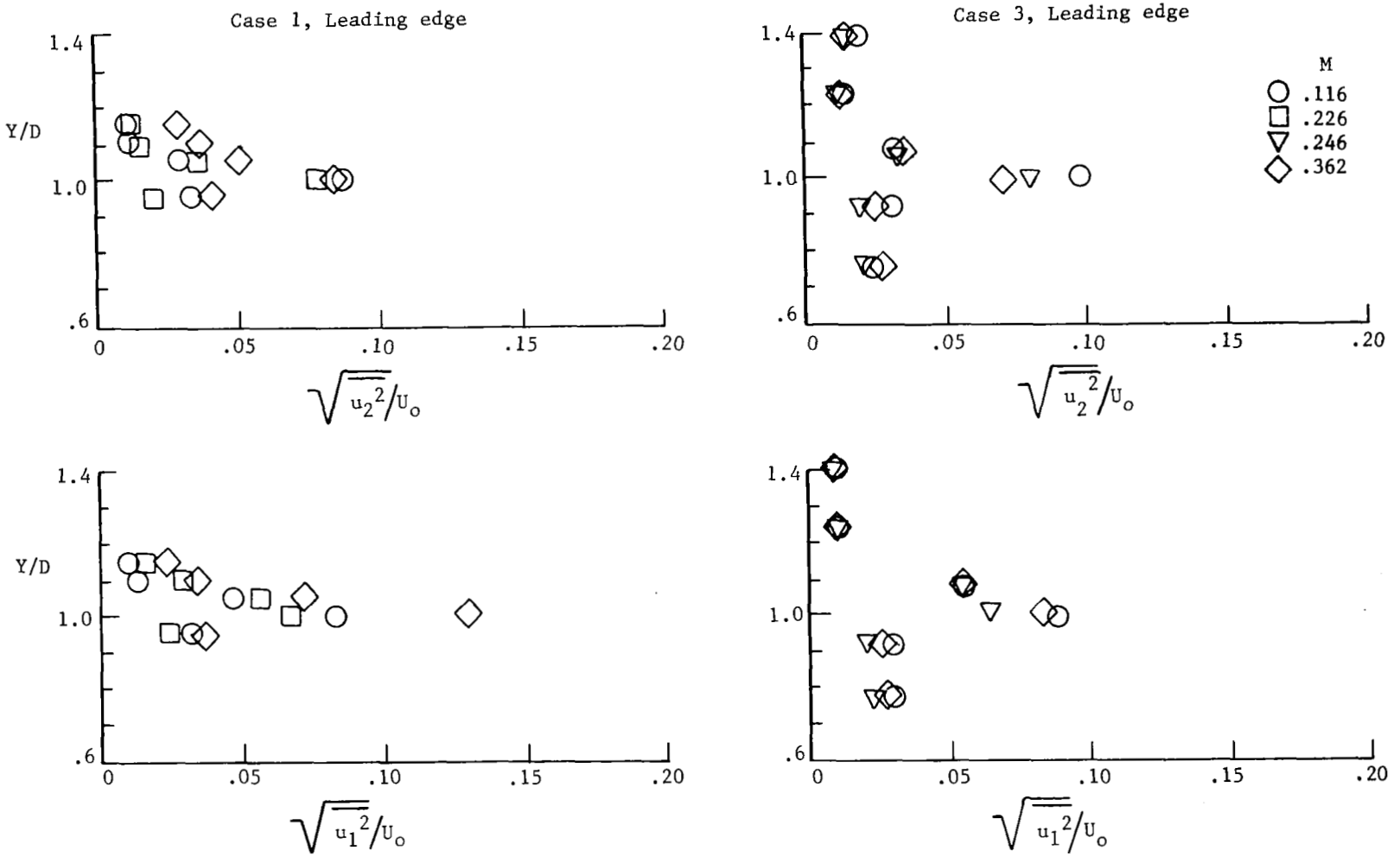

(a) Cases 1 and 3.

Figure 7.- Turbulence intensity profiles.

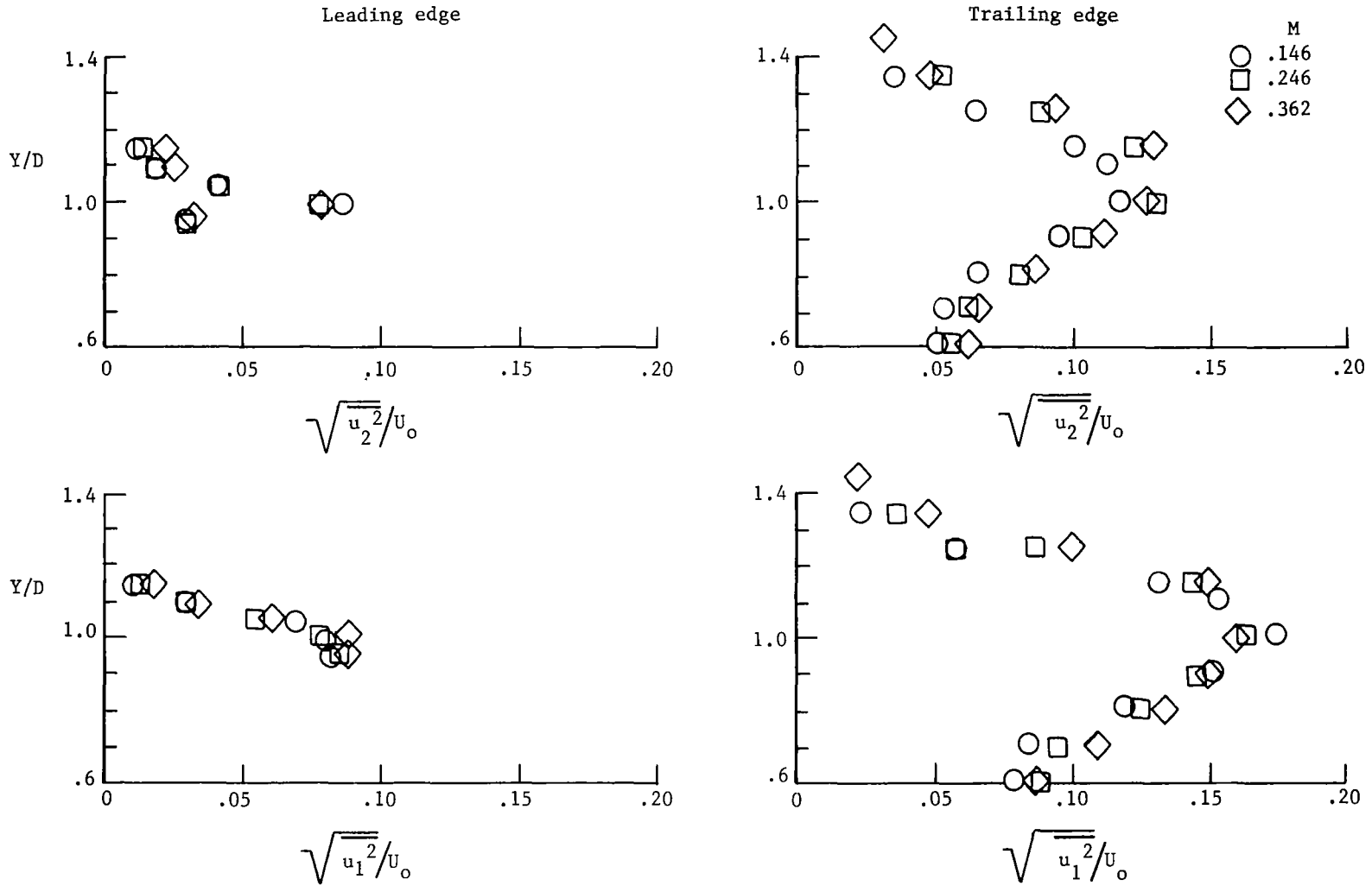

(b) Case 2.

Figure 7.- Continued.

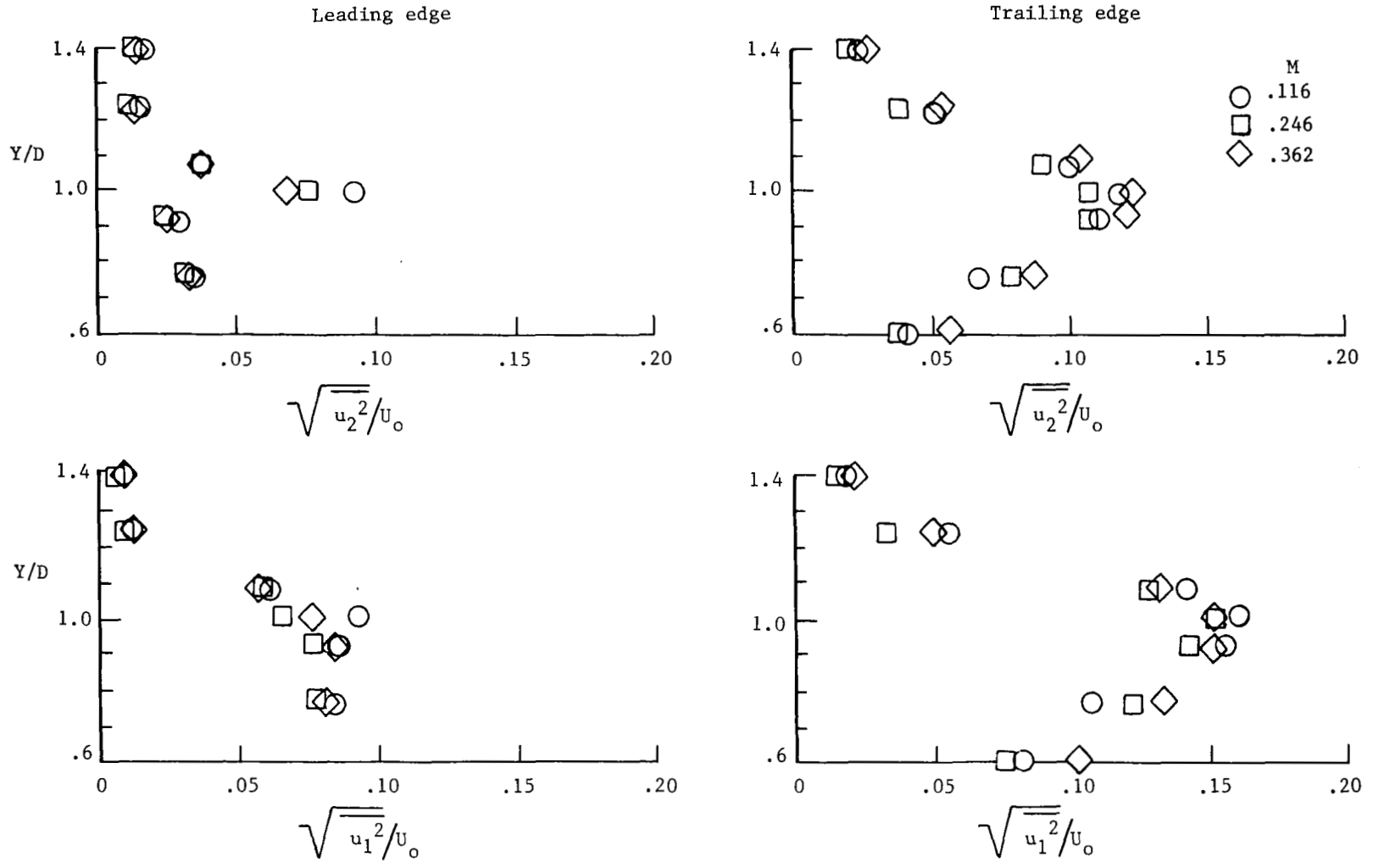

(c) Case 4.

Figure 7.- Continued.

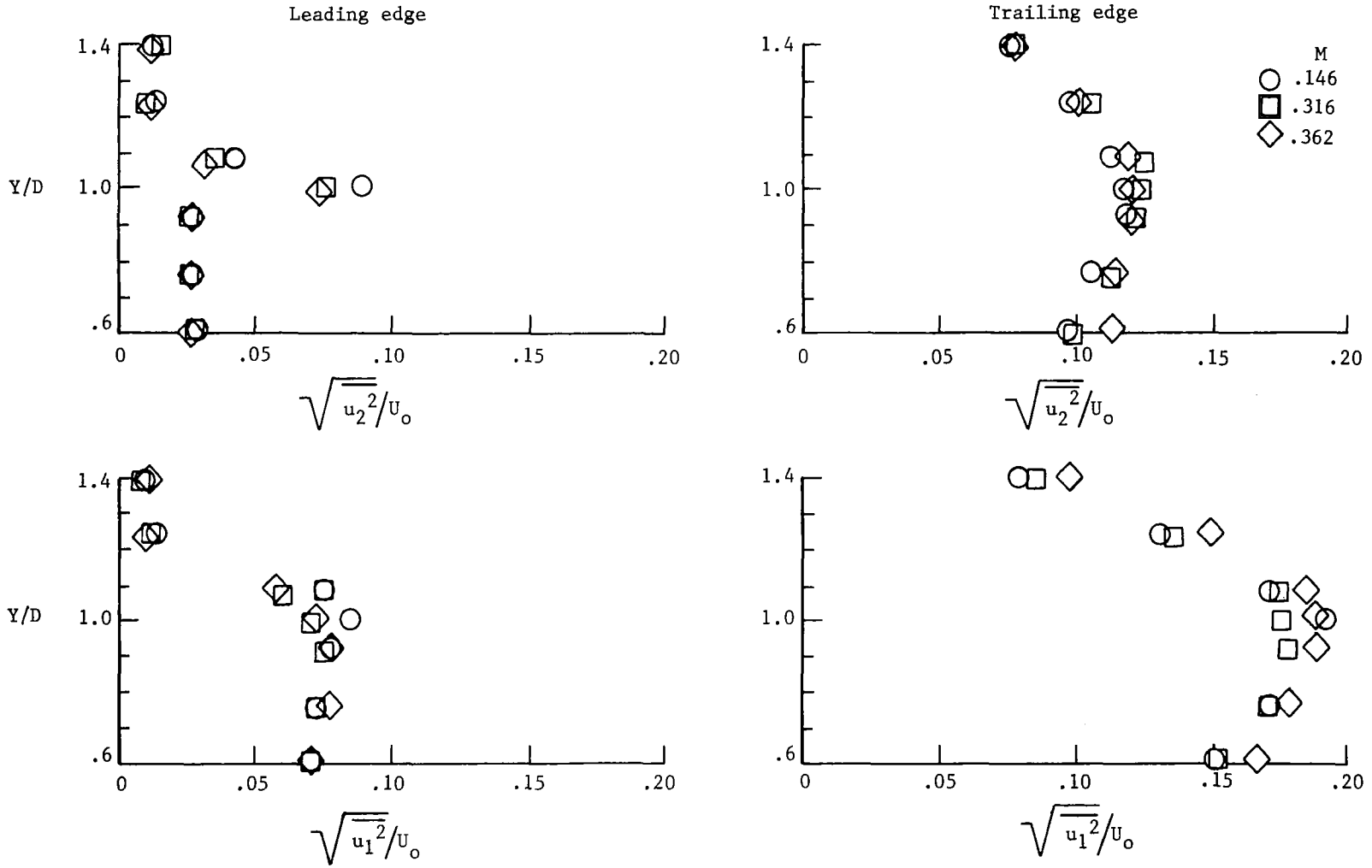

(d) Case 5.

Figure 7.- Concluded.

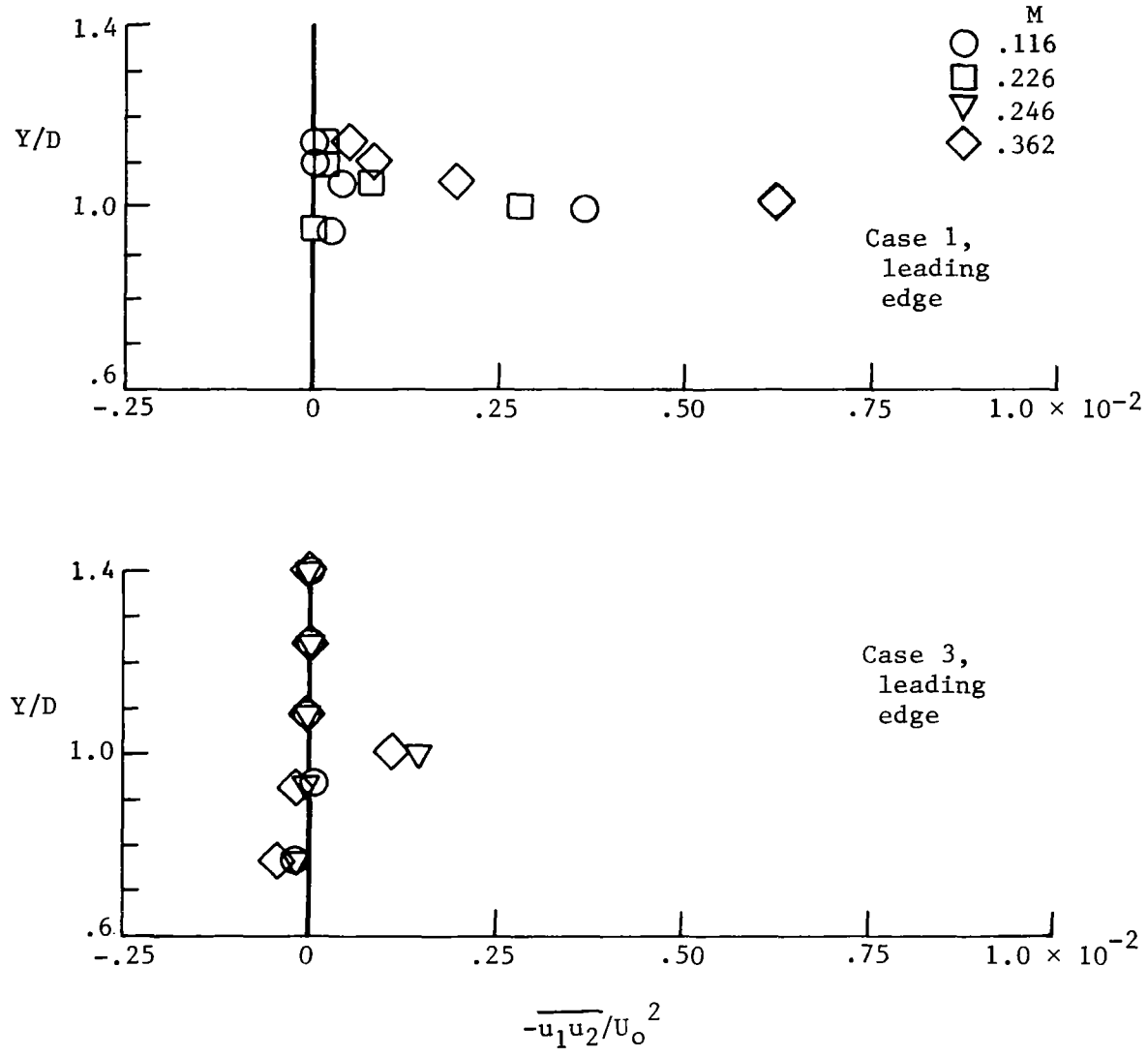

(a) Cases 1 and 3.

Figure 8.- Mean Reynolds stress profiles.

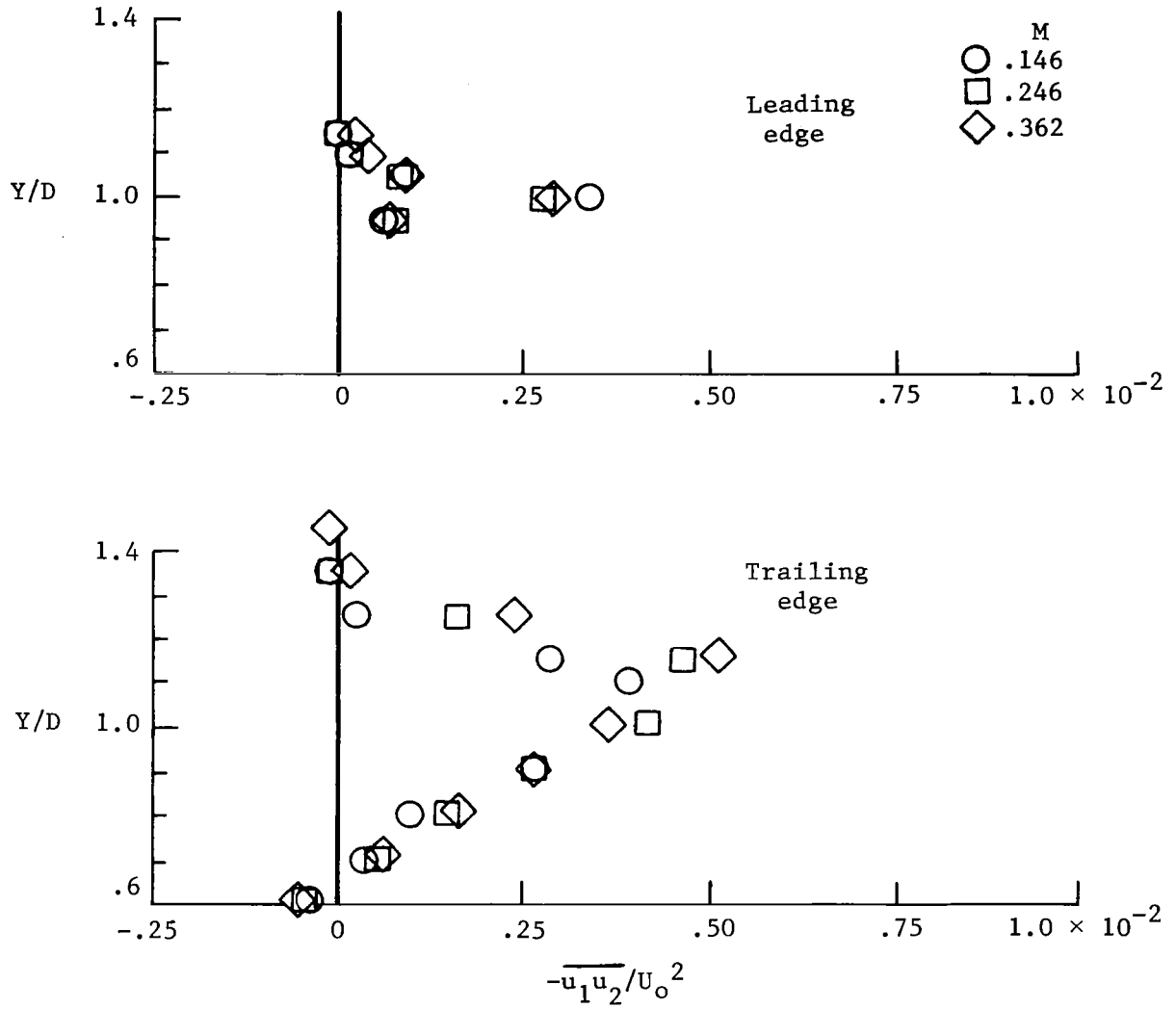

(b) Case 2.

Figure 8.- Continued.

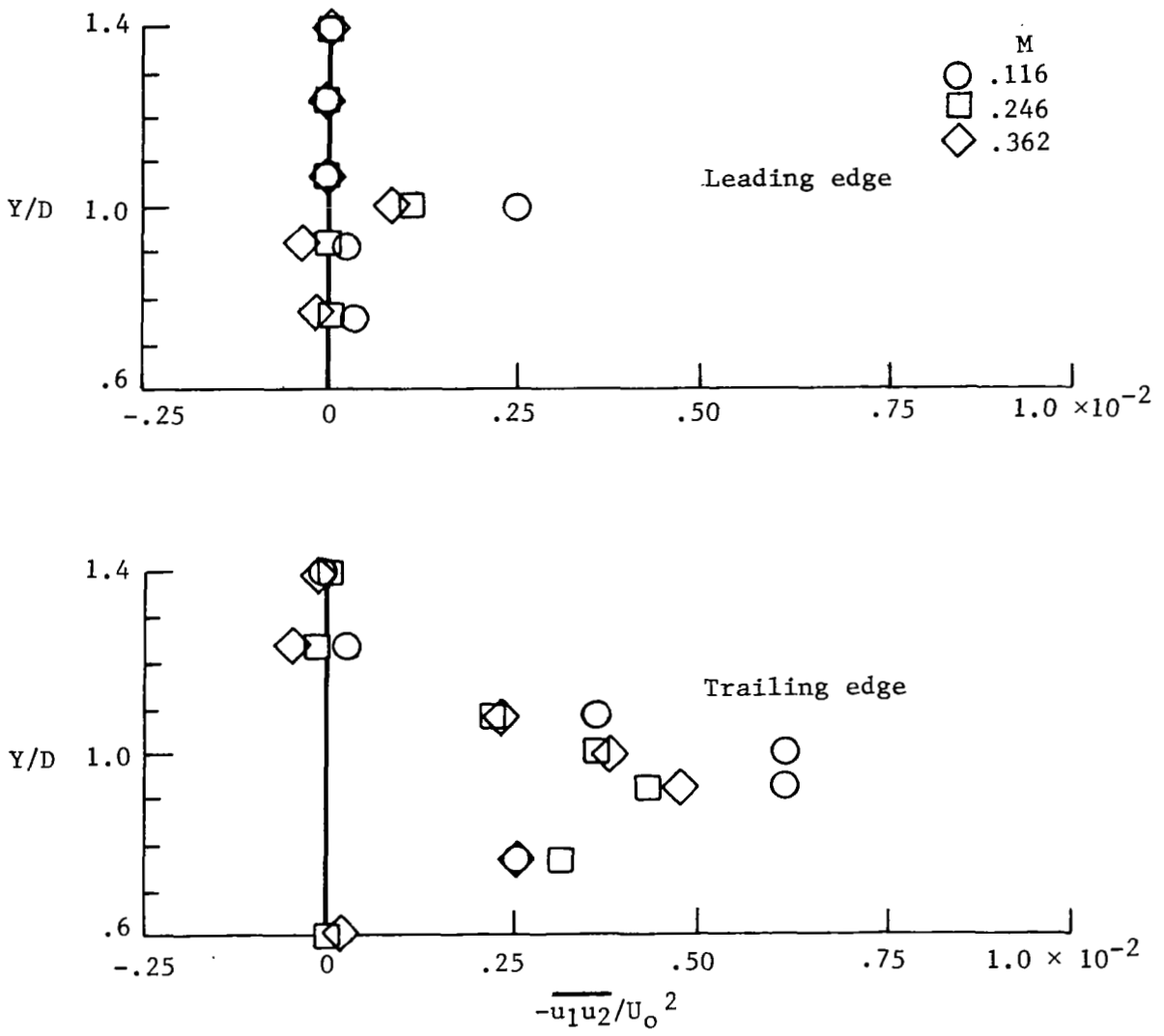

(c) Case 4.

Figure 8.- Continued.

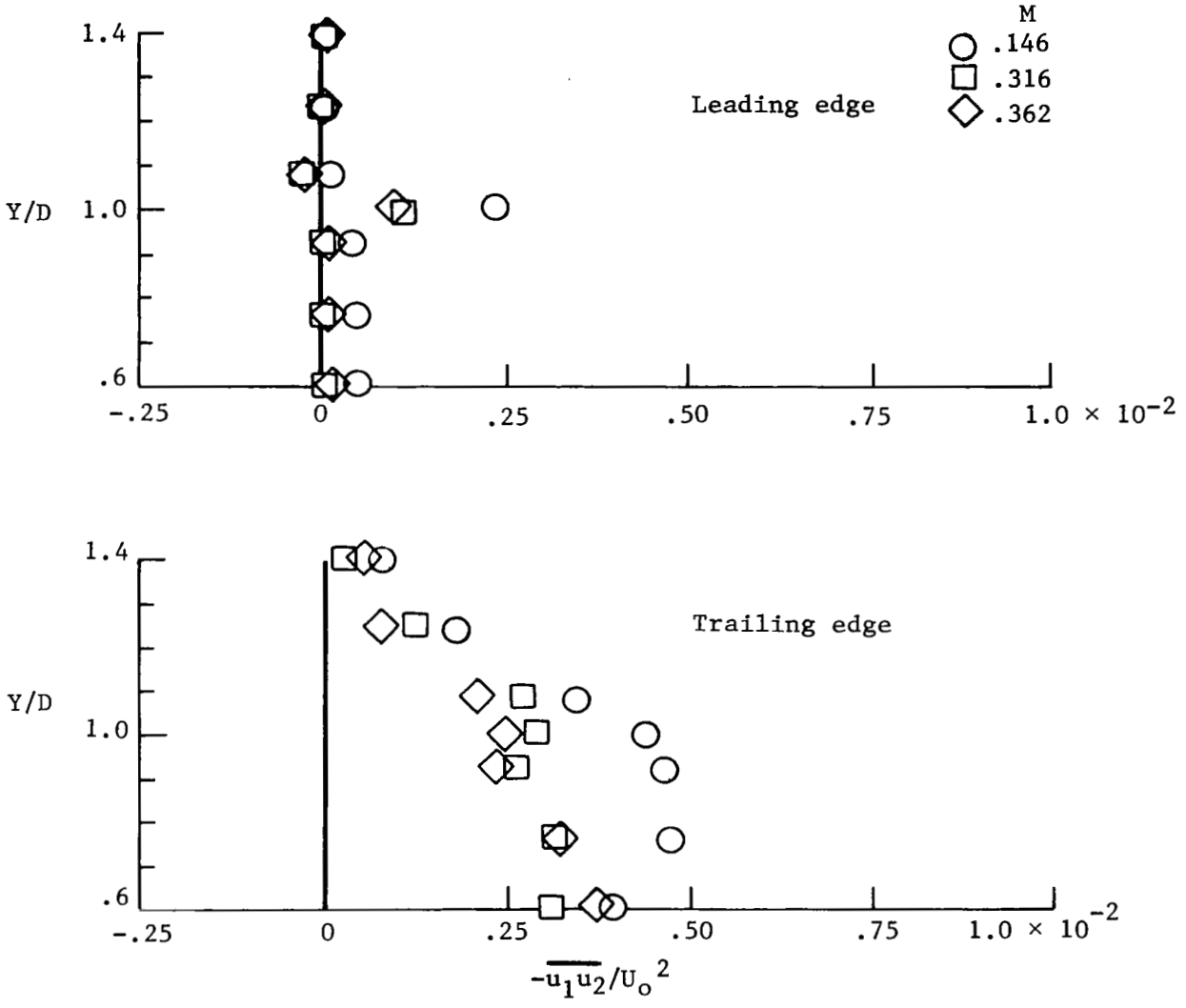

(d) Case 5.

Figure 8.- Concluded.

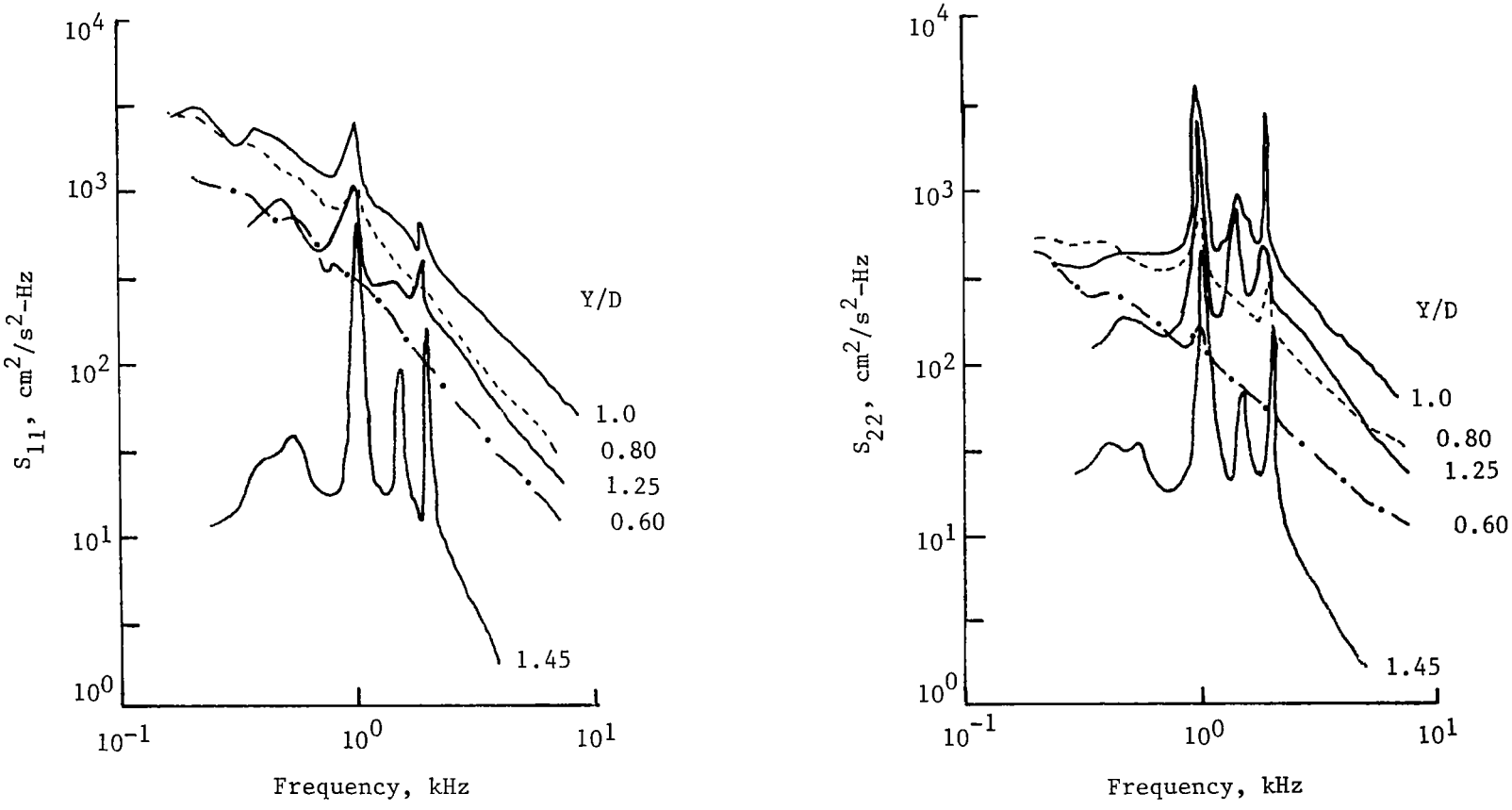

Figure 9.- Velocity spectra at trailing-edge positions for case 2. M = 0.362.

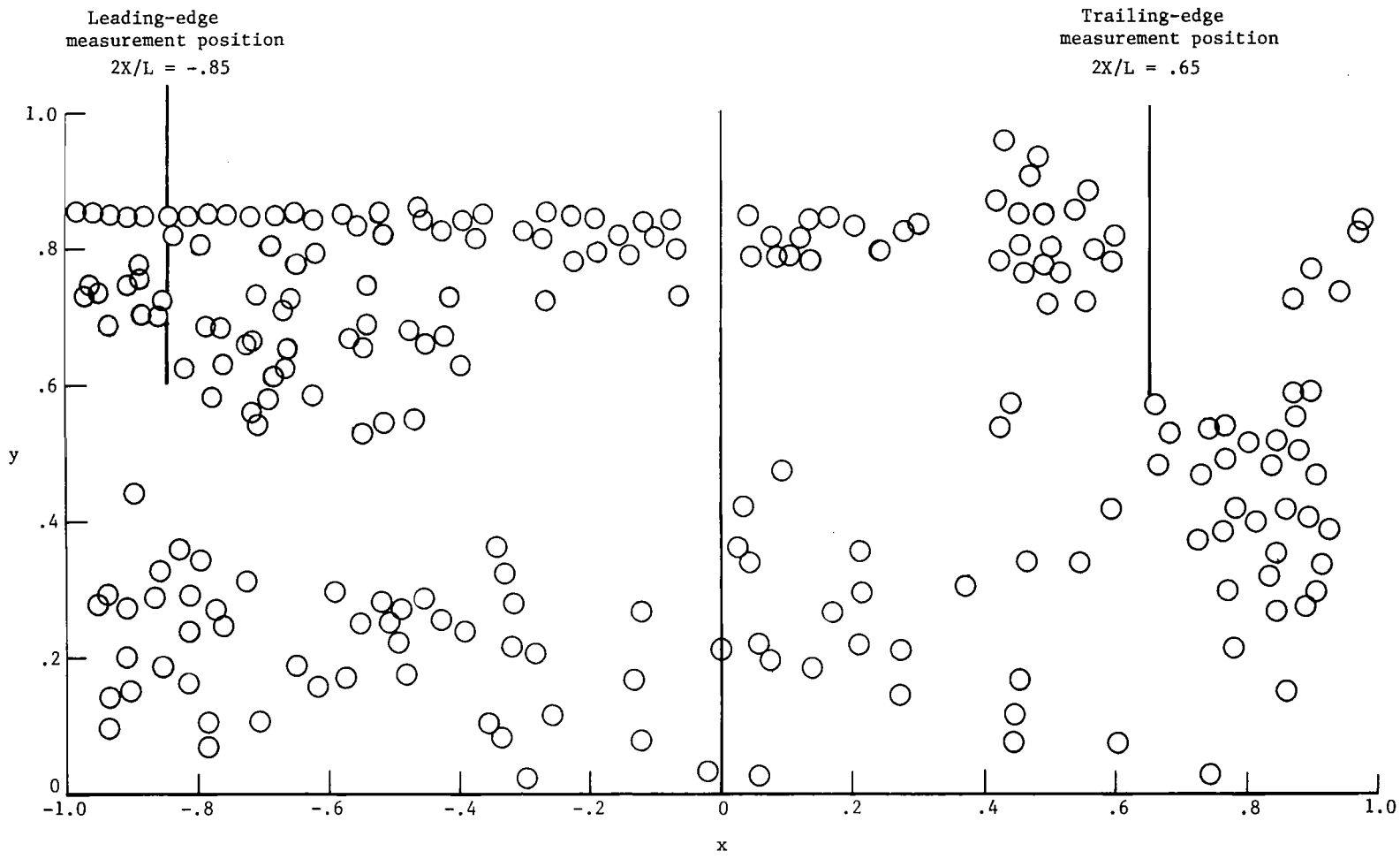

Figure 10.- Instantaneous position of vortices in model.

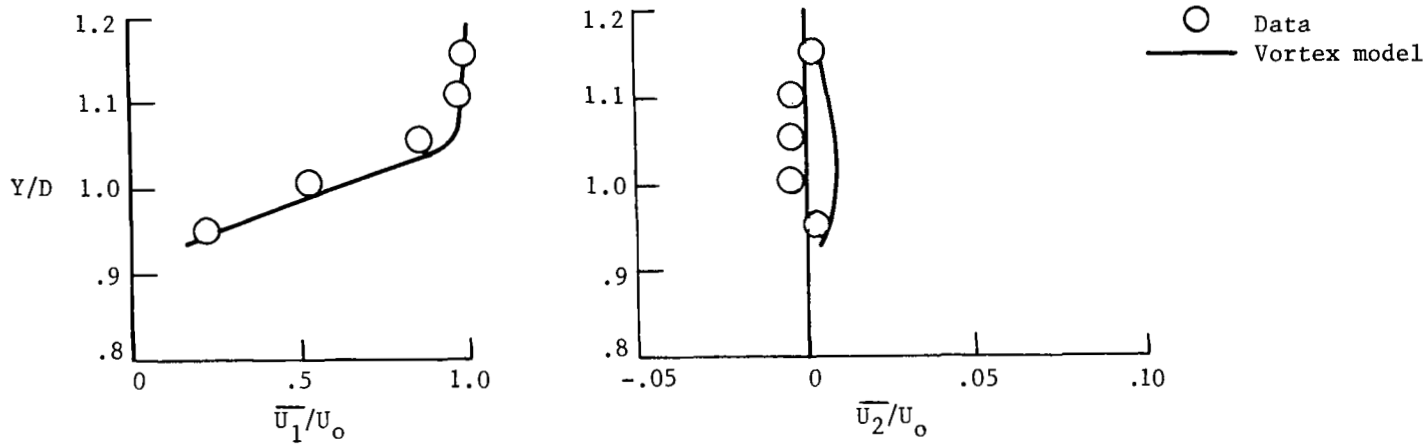

(a) At 2X/L = -0.85.

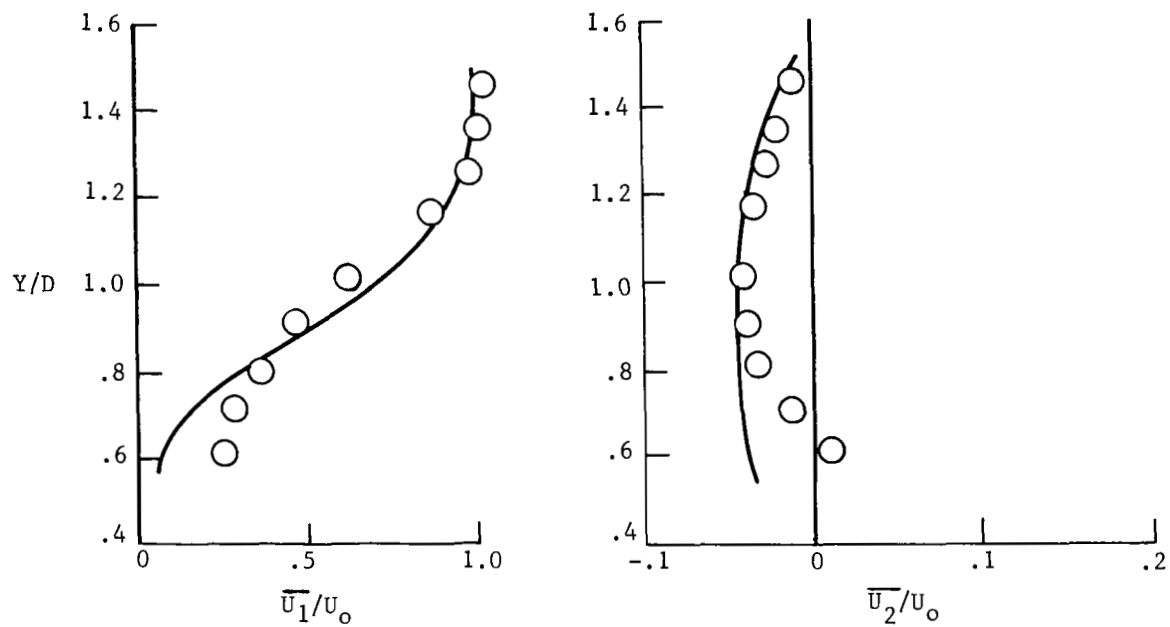

(b) At 2X/L = 0.65.

Figure 11.- Comparison of predicted and measured mean velocity profiles.

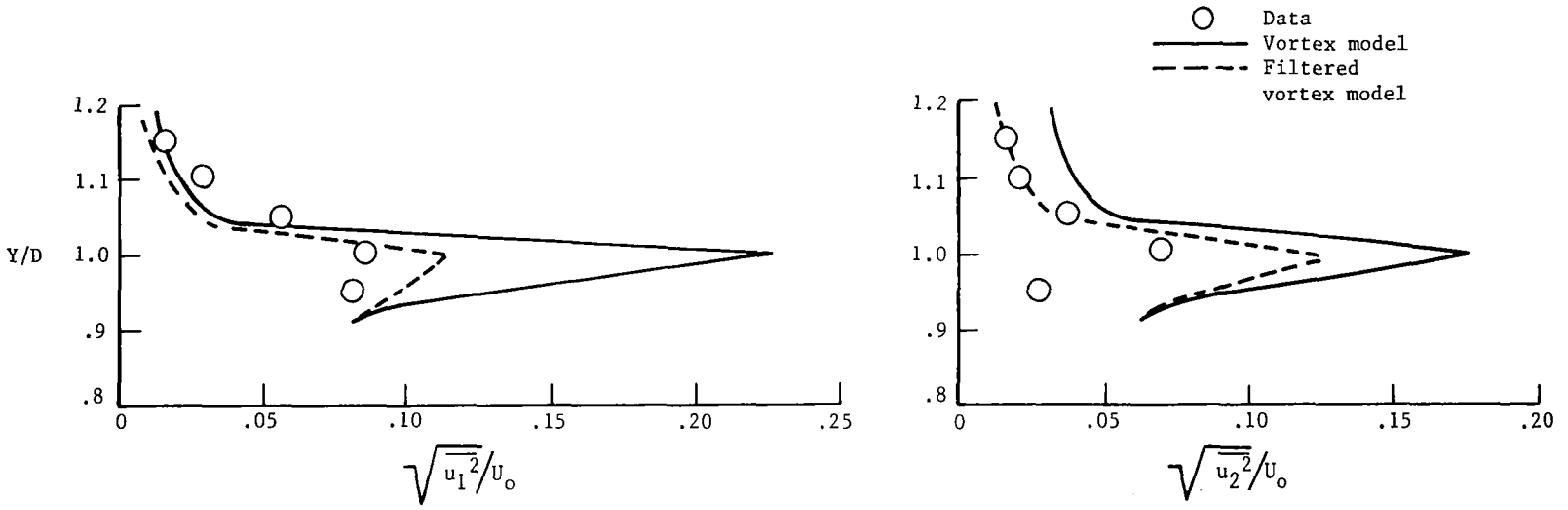

(a) At 2X/L = -0.85.

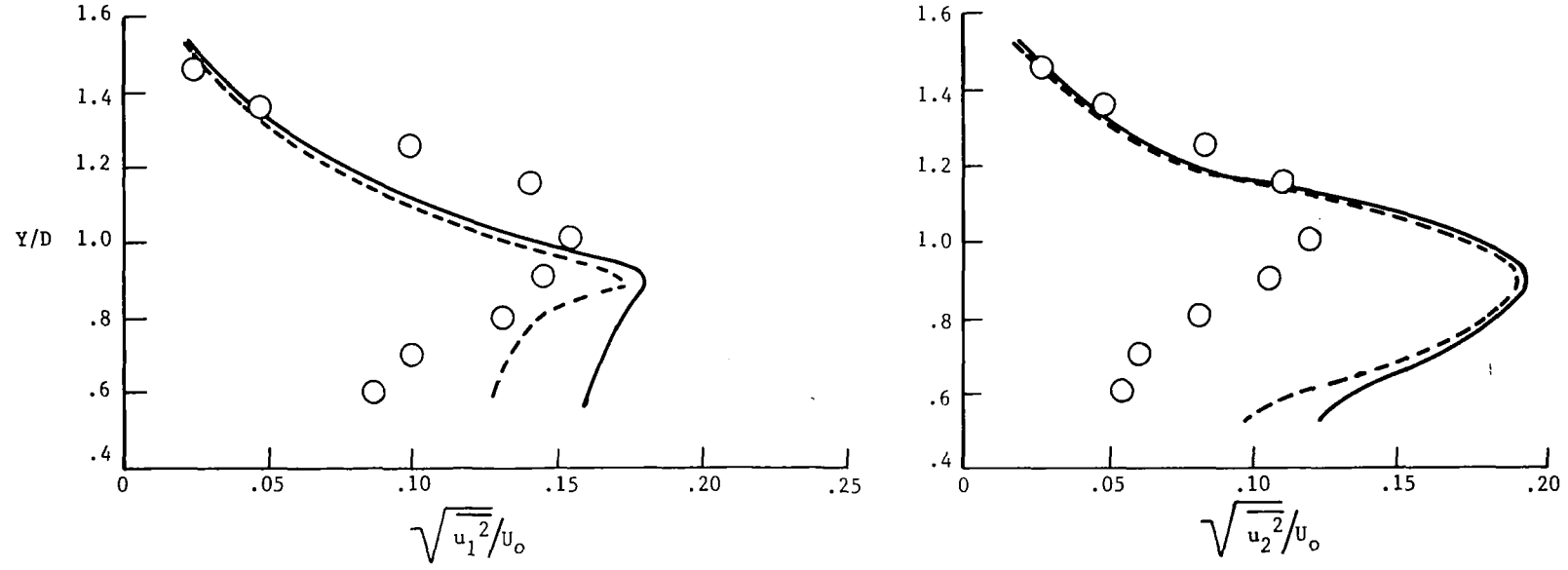

(b) At 2X/L = 0.65.

Figure 12.- Comparison of predicted and measured turbulent intensity profiles.

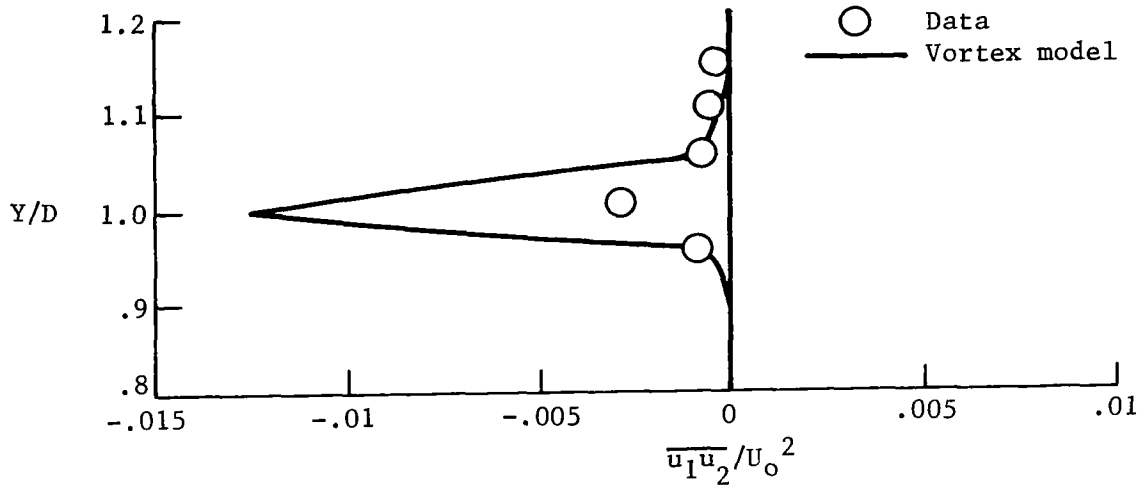

(a) At 2X/L = -0.85.

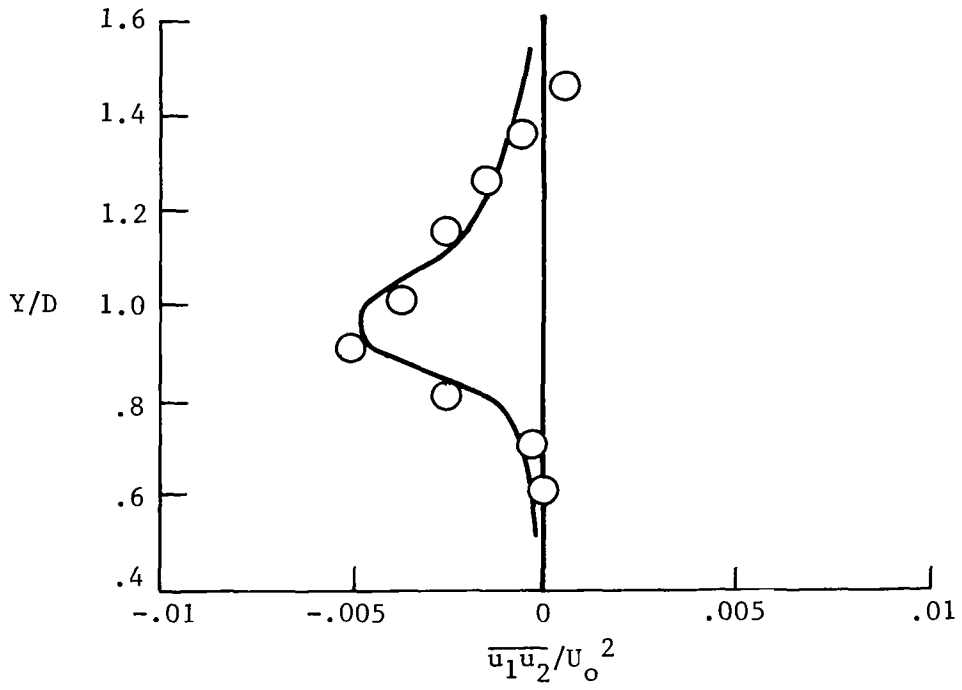

(b) At 2X/L = 0.65.

Figure 13.- Comparison of predicted and measured Reynolds stress profiles.

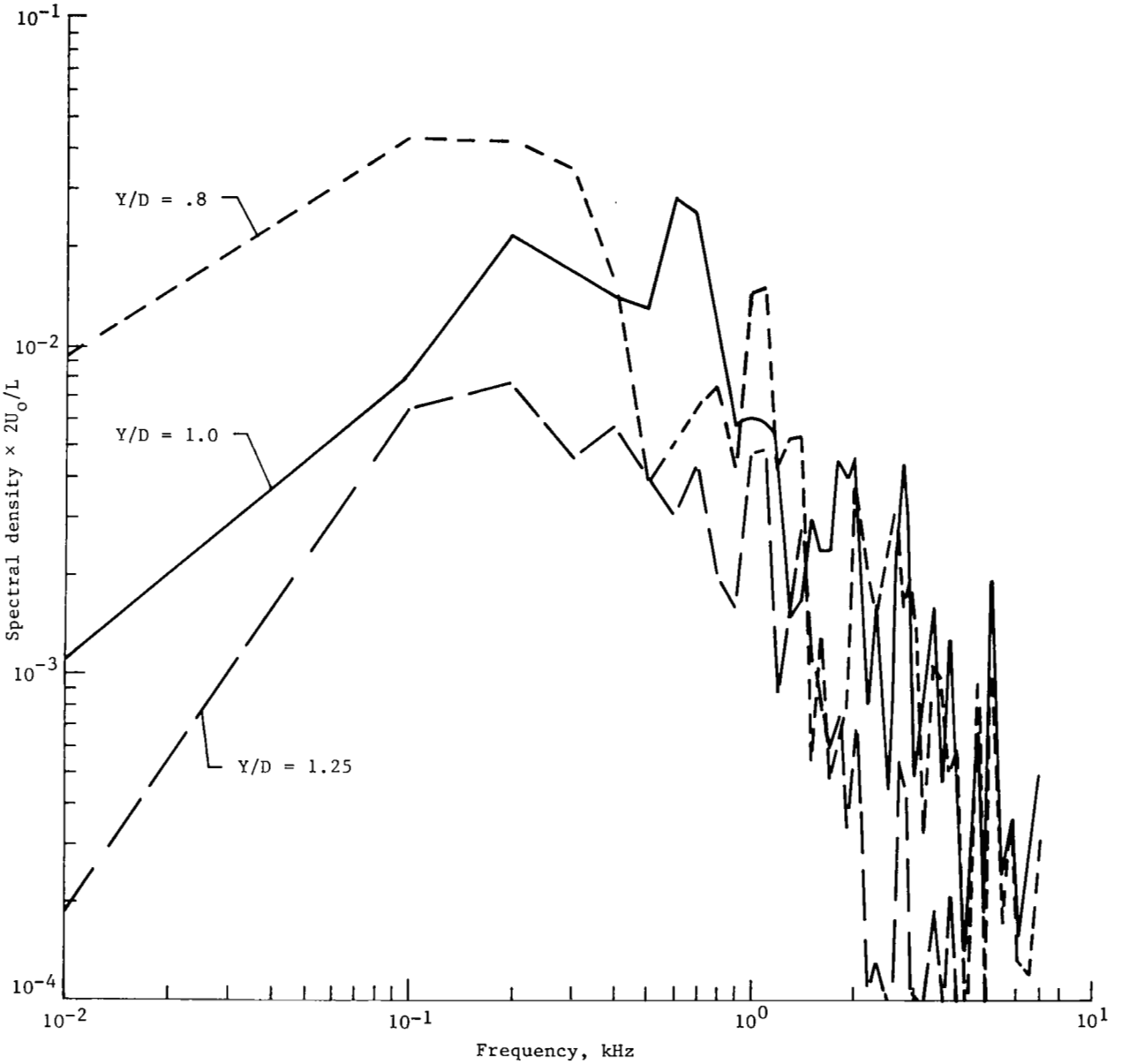

Figure 14.- Spectral density of streamwise turbulent intensity obtained from vortex model results. 2X/L = 0.65.

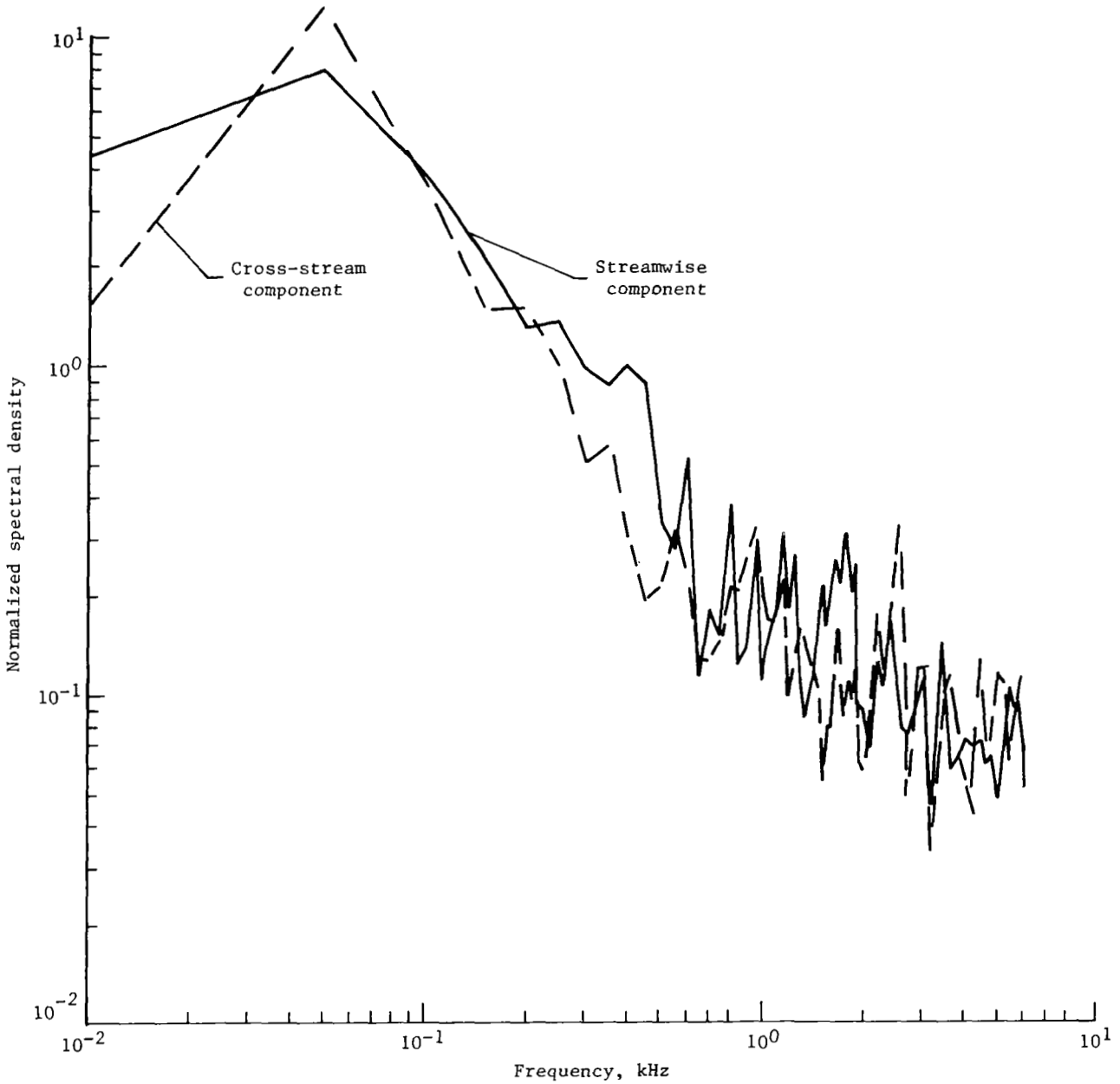

(a) At 2X/L = -0.85.

Figure 15.- Normalized spectral density of turbulent intensity obtained from vortex model results.

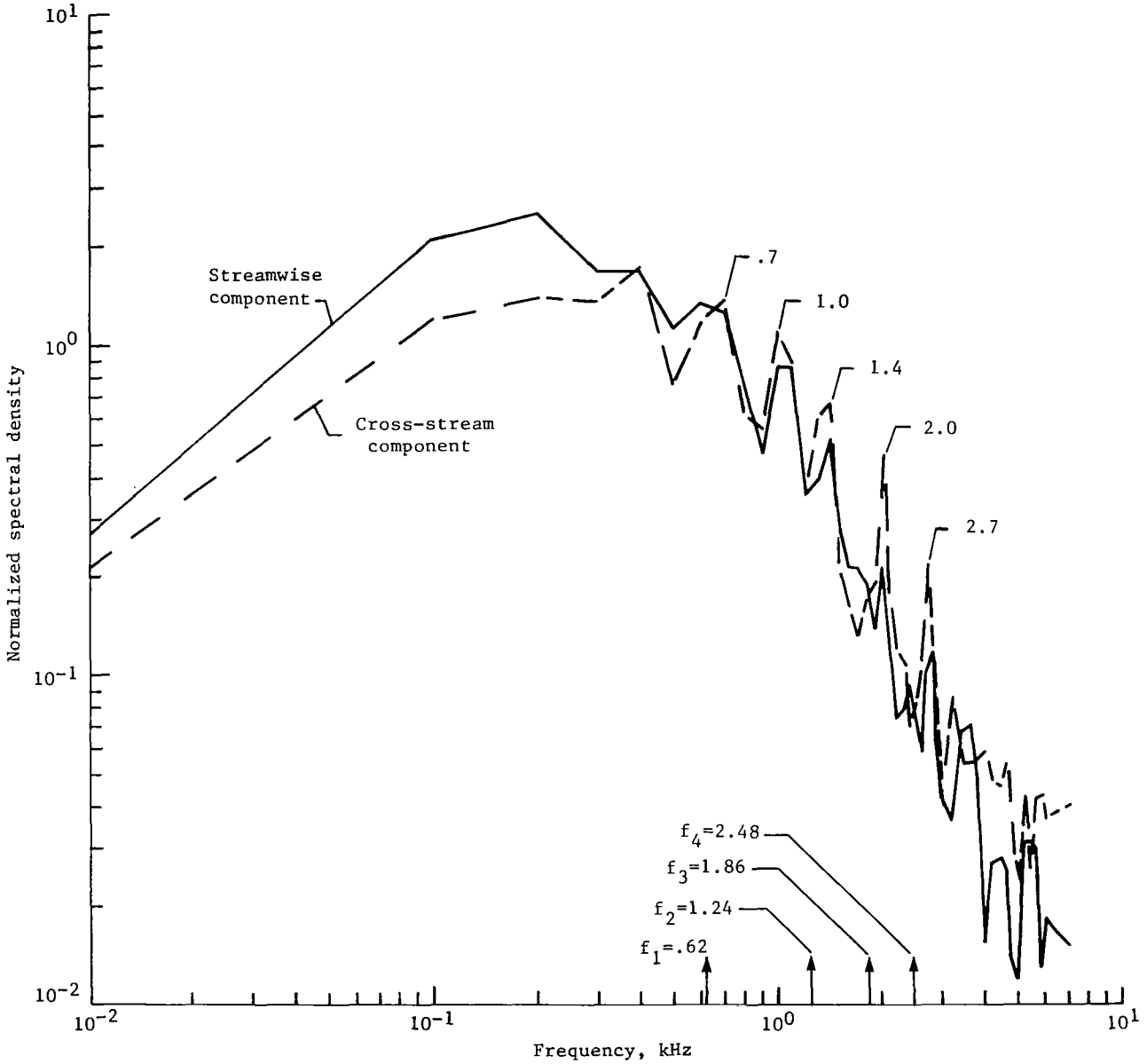

(b) At 2X/L = 0.65.

Figure 15.- Concluded.

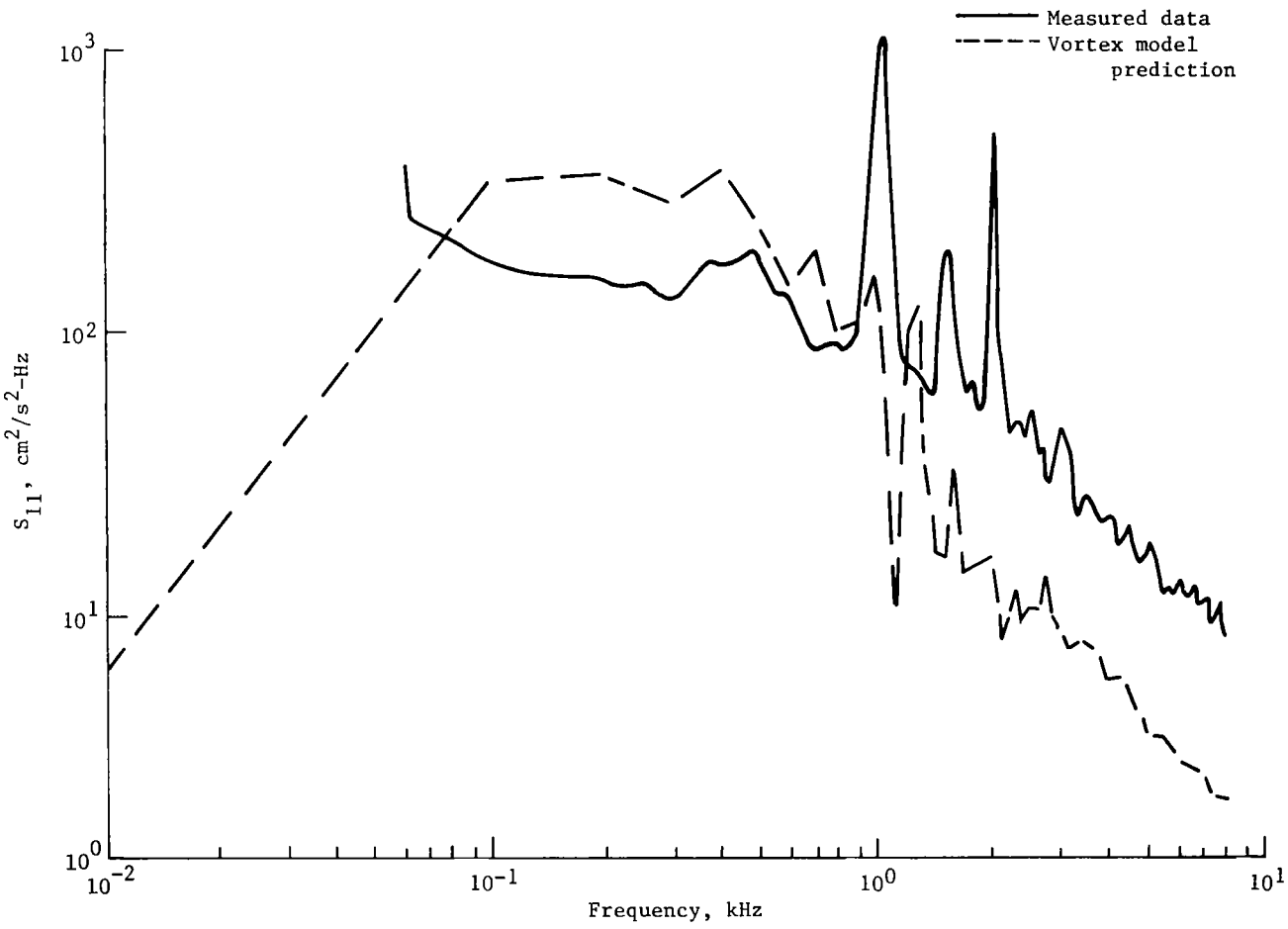

Figure 16.- Comparison of predicted and measured spectral density of streamwise velocity fluctuation at 2X/L = 0.65 and Y/D = 1.35.

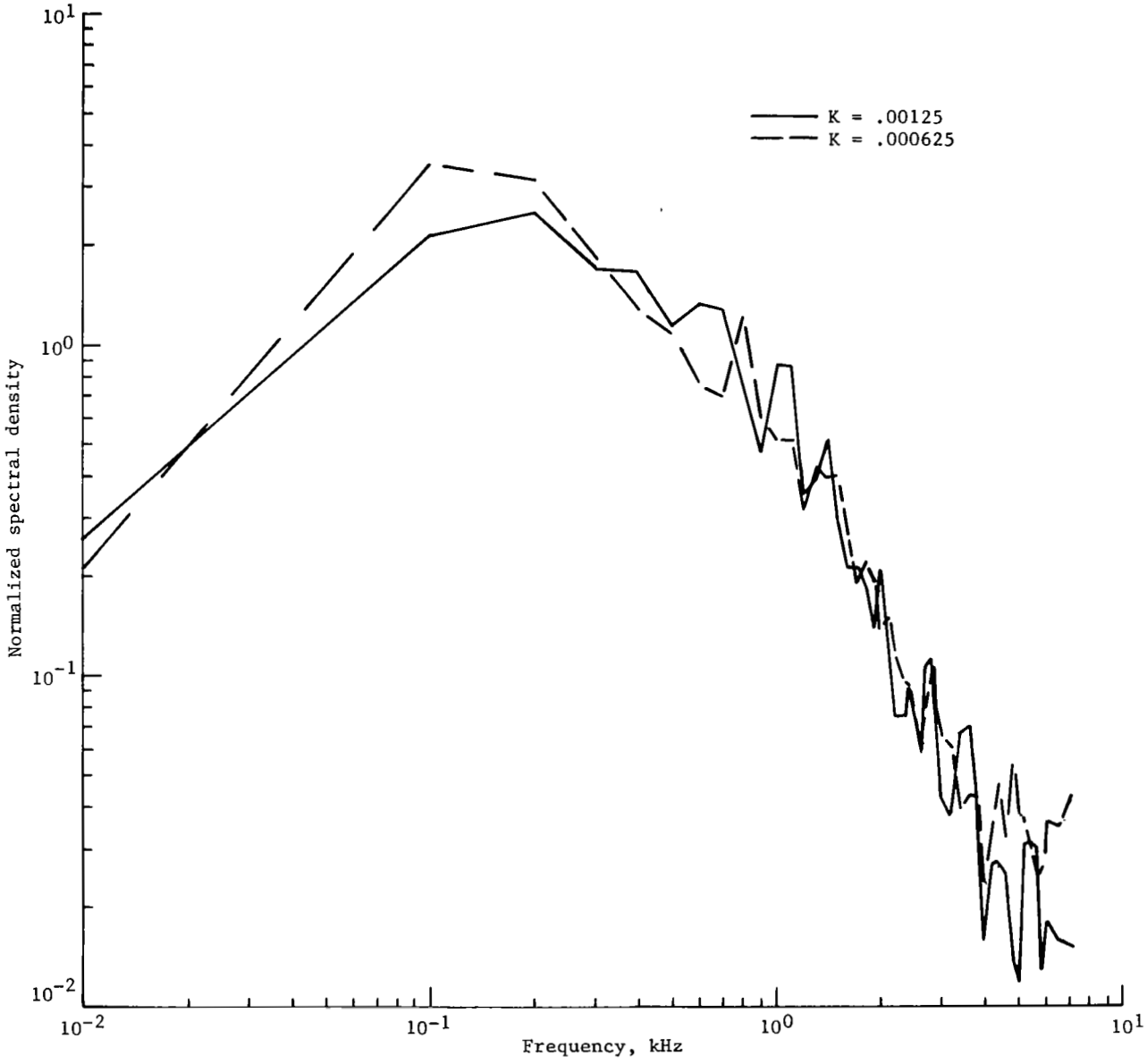

(a) Normalized spectral density of streamwise turbulent intensity.

Figure 17.- Comparison of normalized spectral densities for two values of circulation decay rate K.

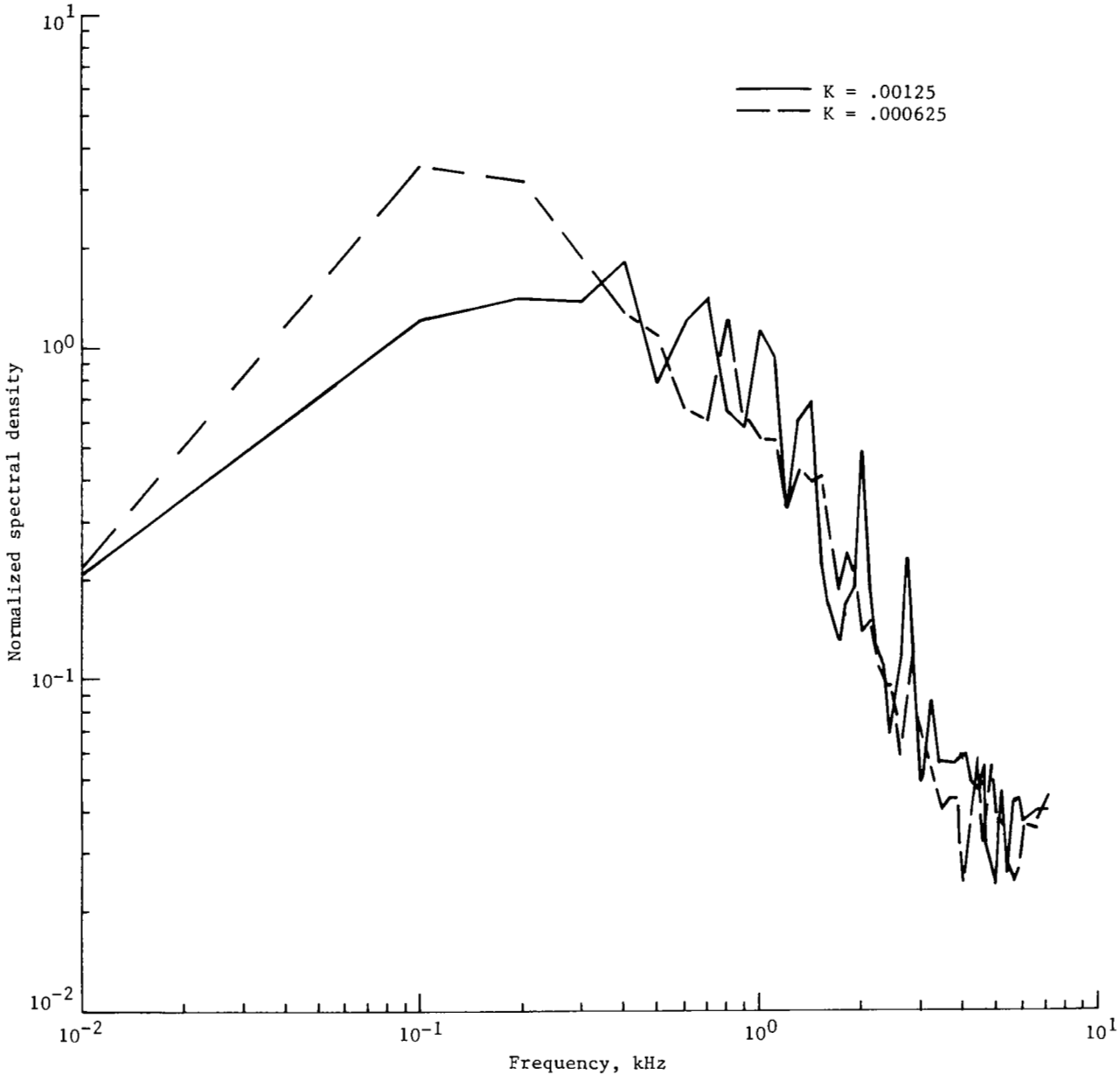

(b) Normalized spectral density of cross-stream turbulent intensity.

Figure 17.- Concluded.

1. Report No.	2. Government Accession No.	3. Recipient's Catalog No.
NASA TP-1505		

4. Title and Subtitle	5. Report Date
EVALUATION OF A VORTEX MODEL OF TURBULENT CAVITY FLOW	September 1979
	6. Performing Organization Code

7. Author(s)	8. Performing Organization Report No.
Jay C. Hardin and P. J. W. Block	L-12684
	10. Work Unit No. 505-06-23-01

9. Performing Organization Name and Address	11. Contract or Grant No.
NASA Langley Research Center Hampton, VA 23665	

12. Sponsoring Agency Name and Address	13. Type of Report and Period Covered
National Aeronautics and Space Administration Washington, DC 20546	Technical Paper
	14. Army Project No.

15. Supplementary Notes

16. Abstract

A two-dimensional discrete vortex model was applied to turbulent flow over a cavity at a Reynolds number based on cavity half-length of approximately 5×10^5. These model predictions are compared with new experimental data, both on a time-average and on a spectral basis. The comparisons indicate that the vortex model reasonably reproduces the mean velocity profiles of this complex flow, while the turbulent intensity and Reynolds stress profiles are generally overpredicted in magnitude. Spectral analyses show that the vortex model introduces unrealistic low-frequency power which becomes less dominant as the model becomes more disordered. In this state, the spectral power distribution of the model is nearly in agreement with that of the data being somewhat too low at the higher frequencies and too high at the lower frequencies. The model is also shown to be capable of reproducing the cavity feedback oscillation phenomenon.

17. Key Words (Suggested by Author(s))	18. Distribution Statement
Vortex models Cavity flow	Unclassified - Unlimited Subject Category 71

19. Security Classif. (of this report)	20. Security Classif. (of this page)	21. No. of Pages	22. Price*
Unclassified	Unclassified	44	$4.50

*For sale by the National Technical Information Service, Springfield, Virginia 22161

NASA-Langley, 1979

3 1 1U,H, 090479 S00903DS
DEPT OF THE AIR FORCE
AF WEAPONS LABORATORY
ATTN: TECHNICAL LIBRARY (SUL)
KIRTLAND AFB NM 87117